New Tools for Urban Analysis: A SLAM-Based Research in Venice

remote sensing

MDPI

Article

New Tools for Urban Analysis: A SLAM-Based Research in Venice

Beatrice Tanduo *, Andrea Martino, Caterina Balletti and Francesco Guerra

Laboratorio di Fotogrammetria CIRCE, Dipartimento di Culture del Progetto, Università IUAV di Venezia, S. Croce 191, 30135 Venice, Italy

* Correspondence: btanduo@iuav.it

Abstract: This research proposes a detailed analysis of the potential of MMS (Mobile Mapping Systems), supported by SLAM (Simultaneous Localisation And Mapping) algorithms, performed on a multiscale test field in order to make a concrete contribution to the morphological study of cities. These systems, developed with the aim of acquiring a large number of points in a short time, are able to map the surrounding area and automatically localise themselves in real time in relation to a determined reference system. The analysed area, located in Venice, was divided into three different test fields characterised by typical elements potentially comparable to those of other urban realities. The data were acquired using the LiBackPack C50, Kaarta Stencil and Heron Lite systems and compared quantitatively and qualitatively with data obtained from more traditional surveying techniques. Specifically, the data obtained from TLS (Terrestrial Laser Scanning) surveys, supported by topographic measurements, were the most accurate basis on which to evaluate the accuracy and completeness of the three different MMS devices. The standard deviation values were initially analysed in the final 3D global models using the C2C (Cloud to Cloud) and C2M (Cloud to Mesh) distance calculation methods. Subsequently, the geometric differences were investigated through the extraction of horizontal profiles, and two more specific 2D analyses were carried out: the first inspecting the residual parameters calculated after the Helmert transformation from two sets of control points obtained from the profiles, followed by a local strain analysis. The study of the local deformation parameters allowed us to validate the results obtained and to identify the real limits of these survey instruments. The aim was to make a concrete contribution to the formalisation of an operative protocol for the morphological study of the city, exploiting the potential of these technologies to overcome the differences in scale and the gap between outdoor and indoor spaces.

Keywords: 3D survey; SLAM; MMS; TLS; LiDAR; accuracy evaluation; point cloud

Citation: Tanduo, B.; Martino, A.; Balletti, C.; Guerra, F. New Tools for Urban Analysis: A SLAM-Based Research in Venice. *Remote Sens.* **2022**, *14*, 4325. https://doi.org/10.3390/rs14174325

Academic Editors: Filiberto Chiabrando and Domenico Visintini

Received: 1 August 2022
Accepted: 25 August 2022
Published: 1 September 2022

1. Introduction

The acquisition of three-dimensional data through laser scanning or digital photogrammetry is a well-established documentation technique in a variety of fields, making it possible to carry out analysis in a non-invasive way [1–3].

All survey methods are characterised by their own advantages and limitations, requiring the operator to make choices on the basis of the purpose of reproduction, the scale of reduction, and especially the type of object to be surveyed. Geomatics techniques are used according to their required application, making it possible to perform different analyses using multi-scale approaches by varying the technique and the method of data processing.

Morphological studies have been carried out on many cities over the years. Building typology and urban morphology are two concepts that are related to one another, but which are unfortunately too often investigated separately. Research performed by Alexander Klein, Saverio Muratori and Aldo Rossi shows how the building typology can be identified only in concrete applications, that is, in the building fabric, and that an urban fabric cannot be identified except for in its total form, that is, in the urban organism [4–6]. It is becoming

clear that analysing a city as a whole, in its totality, is the key to understanding and investigating it; the changing nature of a city makes its typological classification difficult, therefore necessitating tools of synthesis and analysis [7,8].

In this context, we propose a methodological protocol able to be used to develop an analytical approach to the study of cities through the techniques of urban survey and the relative comparison between the different metric data acquired. The main purpose of this research is to experiment SLAM survey techniques in order to support urban analysis within the complex urban morphology of Venice.

Venice is undoubtedly a city with an urban structure that is difficult to catch and comprehend, but over the years, it has been the subject of several studies. Giuseppe Cristinelli and Egle Renata Trincanato focused their studies on specific Sestieri of the Island. Both used historical–critical descriptions of the analysed urban areas combined with the orthogonal projection drawings of the main building types, proposing on the one hand a categorisation of the different distributive structures of Venetian building planning with the intention of recognising a common matrix, and on the other a study of the spatial, constructive and functional solutions typical of Venetian social housing [9,10].

In both works, bi-dimensional drawing, integrated with photographic documentation, was the knowledge tool that made the morphological study comprehensible and globally describable. Three-dimensional approaches, thanks to modern survey techniques, are here regarded as the main tools for investigating data inherent to the geometric aspect, the spatiality, and the shape of architectural and urban objects.

This work compares information obtained by cartography, archival sources, and geodatabases of three-dimensional models at the urban scale coming from MMS by means of SLAM algorithms. Different survey methods are experimentally tested and compared, together with the use of modern cartographic tools, ranging from georeferencing techniques to the use of three-dimensional geographic information systems.

Following these considerations, it was decided to focus this research on a particular area of the city: a part of the Sestiere of Dorsoduro, characterised by recent urban transformations.

Related works on the potential of MMS to compete with the more traditional survey techniques are taken into account, as well as the information regarding the data elaboration phase related to SLAM algorithms. An evaluation of the quality and accuracy of MMSs 3D point clouds can be found in [11–13]; experiences on the use of portable mapping systems combined with other survey techniques are described in [14,15]; and comparisons between SLAM surveys and TLS/photogrammetric surveys are well described in [16–19]. Additionally, more specific tests and analyses of the performance of different commercial IMMSs were performed in [20,21], and experiences in the deployment of these systems for the documentation of cultural heritage can be found in [22–26].

Commencing with the state of the art concerning the use of portable LiDAR systems for environmental documentation and metric purposes, this paper aims to propose the use of MMS at both architectural and urban scales, in order to provide a geomatic tool for the morphological study of cities. Applying these surveying techniques, it is possible to study the city in both a planimetric and geometric way, decreasing the time required for acquisition and making it possible to use a multi-scale approach.

One of the innovations of MMS is the ability to merge information regarding both external and internal environments in a single dataset, offering a geomatic solution to the division between the concepts of urban morphology and building typology; the urban component is investigated together with the building component, merging two realities that are usually analysed separately.

In situations where the geometry and configuration of the area under inspection preclude the use of other survey techniques, the application of MMSs is becoming more prominent.

This is the case, for instance, for Venetian canals that are devoid of docks, where it is obvious that it is difficult to perform a laser scan or a conventional photogrammetric survey. This research also looks into the possibility of testing these devices by boat.

Data integration obtained from SLAM technology devices and from the most consolidated survey techniques (topography, GNSS, laser scanning and photogrammetry) is becoming a basis for the provision of innovative tools for the synthesis and analysis of the urban form following a geomatic approach [27].

Test Fields

The analyses were performed within an area including some islands of the Santa Croce and Dorsoduro Sestiere, characterised by the presence of social housing and small buildings.

Over the centuries, the morphological conformation of these architectures has been transformed many times to satisfy the needs of the population. Since 1700, buildings have increasingly begun to lose their individuality, not only externally, but also in terms of their internal distribution [28].

These observations, considered universally valid for the implementation of a morphological analysis of the urban fabric, led to the choice of this area as a test field.

Three different test fields (Figure 1), each defined by specific morphological characteristics, were chosen within this area to be examined in more detail in order to evaluate the results obtained by the MMS devices.

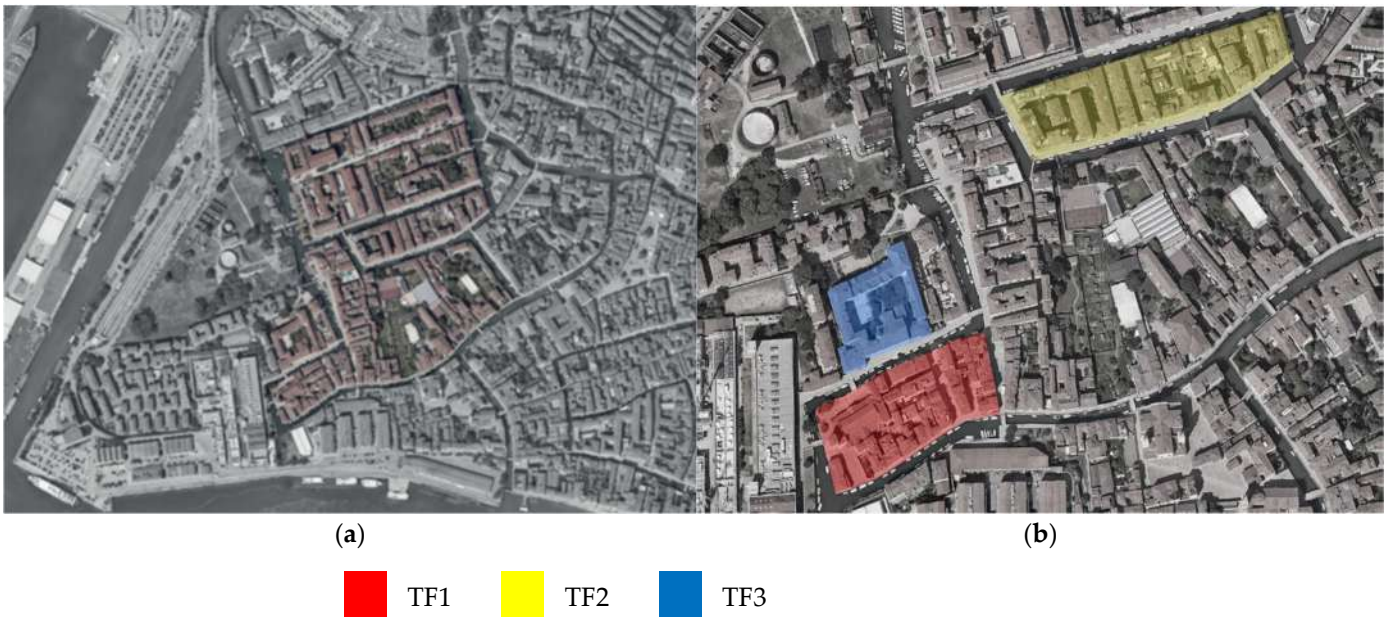

Figure 1. Analysed area (**a**), and Test fields 1, 2 and 3 (**b**).

Test field 1 (TF1) defines the area between the church of San Nicolò dei Mendicoli and Calle Riello. When choosing this area, it was considered that the presence of the narrow irregular streets opening into larger spaces could be a characteristic easily attributable to any urban reality. One of the analyses carried out here concerned the ability of MMS to acquire information related to the highest facades and the narrowest streets.

Test field 2 (TF2) includes the entire island of Cereri. The narrow and long insula, urbanised since 1500, is a typical example of Venetian popular housing. This test field is more regular in its conformation, despite the rhythmic and volumetric variety that characterizes the facades. This insula was mainly chosen as a test field to estimate the accuracy of MMS in the acquisition of information over long periods of time at long distances.

Test field 3 (TF3) covers the areas related to the entrance, the cloister and the indoor spaces of the Terese headquarters of Università IUAV di Venezia. Here, the effectiveness of the instruments at negotiating the dynamic transition between urban and architectural scales and between outdoor and indoor spaces was analysed.

During a single SLAM acquisition performed from a boat, the entire area was also examined.

2. Materials and Methods

The survey and representation of architectural and urban heritage have always been among the main purposes of geomatics. A series of surveying techniques, characterised by the combination of different sensors and devices for data storage, transmission, and treatment, makes it possible to obtain extremely detailed representations, from which it is possible to obtain useful information for the study of urban morphology [29].

2.1. Topographic and GNSS Survey

Three topographic survey campaigns (Figure 2) were carried out using the Leica TCR1103 total station: for TF1, two small isolated networks were arranged, the first one consisting of an open polygon constrained at the extremities (6 cornerstones and 30 detail points), the second one consisting of an isostatic triangle (3 cornerstones and 22 detail points); for TF2, a larger network (20 cornerstones and 248 detail points) was created.

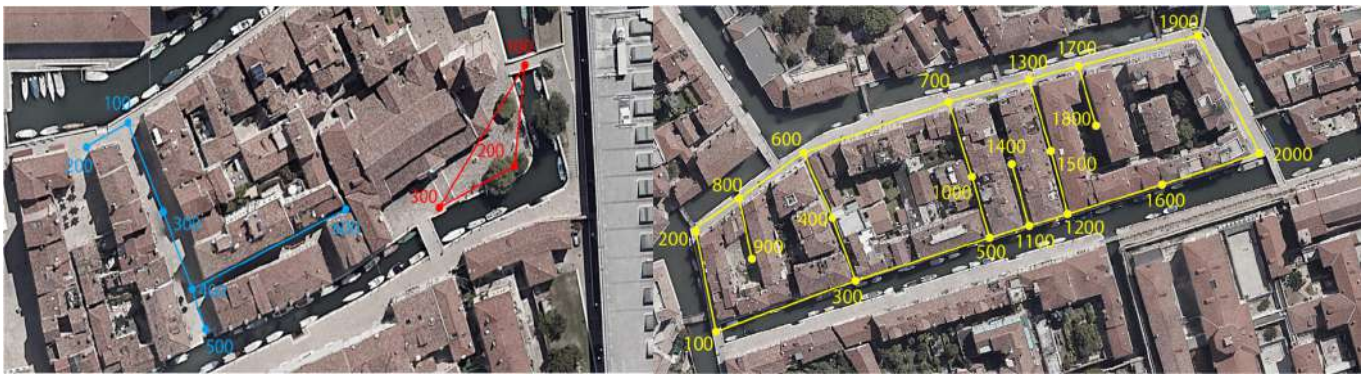

(**a**) (**b**)

Figure 2. Topographic survey campaigns: TF1 (**a**) and TF2 (**b**).

The observations were subsequently processed by least-squares computation using MicroSurvey StarNet software (Version 9.0, MicroSurvey Software Inc., West Kelowna, BC, Canada) to obtain the adjusted coordinates of the surveyed points and the standard deviation of each one.

Using the topographic network reference stations, a GNSS survey was carried out by means of the Stonex S900 satellite (STONEX Srl, Paderno Dugnano, Italy) receiver set on nRTK differential positioning measurement mode. The use of a single receiver to collect RTCM corrections from a network of GNSS permanent stations made it possible to quickly determine the coordinates of 21 points in the Roma40 geodetic reference system with an accuracy better than 4 cm.

2.2. Laser Scanning Survey

A laser scanning survey campaign was performed using two FARO FOCUS 3D CAM2 S120 phase-difference TLS instruments. The parameters set on the instruments during the acquisition phase guaranteed a measurement accuracy of 6 mm at 10 m; it was therefore decided to maintain a distance of 10 m between one acquisition and another.

Four TLS survey campaigns (Figure 3) were carried out: for TF1, there were two different campaigns characterised by six scans, respectively; for TF2, seventy-one scans were carried out; and for TF3, eleven scans were performed.

(**a**) (**b**) (**c**)

Figure 3. TLS survey campaigns: TF1 (**a**), TF2 (**b**) and TF3 (**c**).

Starting from the individual scans acquired, the processing phase of the dataset made it possible to obtain the final products usable as "Ground Truth" for the extraction of metric and geometric information.

The georeferencing phase of the point clouds within the topographic reference system was performed using the FARO Scene software package. Then, using the CloudCompare software package, the four discrete models obtained were processed by means of the following steps: filtering, resampling, meshing, model optimisation, texturing, and extraction of geometric information.

2.3. MMS Survey

In recent years, the approach to urban and architectural surveying has been increasingly influenced by technological innovation. With respect to urban surveying, the SLAM approach has made a substantial contribution to the morphological study of cities.

SLAM technology, implemented on MMS devices, is based on algorithms that are able to simultaneously map the built environment and to determine the position of the device within that environment. The term "localisation" denotes the estimation of the position and orientation of a sensor with respect to a given reference system, as well as the reconstruction in real time of the trajectory travelled by the device/sensor itself; the term "mapping" refers to the acquisition and digitisation of the surveyed objects [30,31].

An MMS system is essentially "a moving multi-sensor system which surveys the surrounding environment in a kinematic manner" [32], which can be defined as a mobile laser scanner; it is composed of one or more laser sensors, an IMU (Inertial Measurement Unit) consisting of three gyroscopes and three accelerometers, a PC and, in some models, a GNSS receiver, to which a camera is eventually associated for the recognition of 2D features and/or for the acquisition of radiometric values.

Depending on the characteristics of the surveyed area, different types of MMS systems are used, and these can be divided into two categories: the traditional type is installed on vehicles such as cars, boats or aircraft, and which are suitable for surveying large areas, while the other type is transportable by the operator, and can be placed inside backpacks or be handheld, thus permitting the acquisition of narrow passages and indoor scenarios [33].

2.3.1. Analytical Operating Principle

Exploiting the equation proposed in 1996 by Schwarz and El-Sheimy for MMS systems, it is possible to derive an equation that considers the six degrees of freedom of a laser scanner sensor and investigates the position r_i^{gcs} of a generic *i-th* point with respect to the chosen global coordinate system (GCS) [34]:

$$r_i^{gcs} = r_{gnss/ins}^{gcs} + R_{ins}^{gcs}\left(R_{tls}^{ins}R_b^{tls}r_i^b + a_{tls}^{ins}\right) \quad (1)$$

where

- r_i^{gcs}: position of the *i-th* point with respect to the chosen global coordinate system (GCS);
- $r_{gnss/ins}^{gcs}$: position of GNSS/INS sensors in the global coordinate system (GCS);
- R_{ins}^{gcs}: rotation matrix from the Inertial Navigation System (INS) reference system to the Global Coordinate System (GCS); the rotation angle is measured by the three gyroscopes of the Inertial Measurement Unit (IMU);
- R_{tls}^{ins}: rotation matrix from the laser scanner system (TLS) to the inertial navigation system (INS); the rotation angle is estimated during the instrument calibration procedure;
- R_b^{tls}: rotation matrix from the laser beam (b) to the entire laser scanner system (TLS);
- r_i^b: laser beam on the *i-th* point;
- a_{tls}^{ins}: position of the laser system (TLS) relative to the inertial navigation system (INS).

The r_i^{gcs} position of the generic *i-th* point in the global coordinate system is inevitably affected by all the errors that characterise each term of the equation, whose combined effect is propagated, precisely, in the final result.

The estimation of the final error can be conducted by considering, independently, the individual errors given as a contribution by each parameter:

- The accuracy of the LiDAR sensors generally present on MMS systems is ±3cm, and the error on the generic *i-th* point detected by the laser beam increases with increasing distance between the detected point and the sensor;
- Inertial navigation systems implement microelectromechanical components (MEMS) that have limited accuracy;
- The position of the MMS system provided by the GNSS receiver becomes inaccurate if the number of satellites "visible" to the device is reduced as a result of obstructions such as the presence of vegetation and/or buildings.

The integration of GNSS and INS data, solved by procedures based on the Kalman filter, makes it possible to finalise the position estimation of the MMS system; the absolute position acquired by the GNSS receiver overcomes the errors of the INS measurements, while the relative position of the inertial platform counterbalances the low quality or lack of GNSS data [35].

In the SLAM acronym, the term "simultaneous" is meant both in the sense of "synchronous" and in its meaning concerning the "automatic" character of the procedure; although the task of detecting the position of the device within the coordinate system is handled by the GNSS receiver and the IMU, the contribution of LiDAR and/or imaging sensors (which are able to recognise common 2D features in two scans performed in two consecutive temporal instants t_0 and t_1) to the resolution of localisation problems has to be pointed out, and the integration of data derived from mapping devices to those obtained from navigation sensors allows the improvement of the mapping itself, and therefore of the final result.

Post-processing of the data using dedicated software optimizes the final solution, both quantitatively and qualitatively [36]. To minimise errors in the final cloud, the MMS system proceeds by splitting the entire point cloud into n "virtual" static scans, each performed at a temporal instant t and at a given spatial location, and applying analytical procedures to each scan on the basis of the ICP algorithm. This algorithm can solve geometric dissimilarities and misalignments between two consecutive scans by estimating R_j and R_k rotations and t_j and t_k translations that minimise the sum of the squared error computed on the distance between the homologous points m_j and m_k belonging to each pair of clouds using the following equation [37]:

$$E = \sum_{j-k} \sum_{i} \left| \left(R_j m_j + t_j \right) - \left(R_k m_k + t_k \right) \right|^2 \quad (2)$$

Moreover, it is recommended that the beginning and the end of the survey path coincide, so that the first and the last scans overlap; in this way, the recognition of an adequate number of homologous points m_j and m_k between the scans that open and close

the survey project will enable the redistribution of the residual error gathered by every scan alignment, avoiding the occurrence of drift errors [38].

The study of the analytical principle and the considerations reported in this section were taken into account in the data acquisition phase in order to minimise deformations and misalignment errors in the final point cloud. A "loop closure" approach to the survey paths was adopted every time to avoid drift errors: to achieve greater satellite coverage, and to allow the GNSS receiver to better estimate the absolute position, the operator avoided walking near taller buildings insofar as this was possible, and a regular stride has been maintained, avoiding sudden changes in direction, in order to allow better IMU platform performance, a more accurate estimation of the motion model, and hence the correct application of the Kalman filter technique. In particular, with respect to the indoor spaces of TF3, an increased number of acquisitions of the same places were made, in order to allow the feature track camera to recognise a proper number of common 2D features in consecutive scans even when the lighting in the room was very low.

2.3.2. MMS Acquisition Phase

Three different MMS (Figure 4, Table 1) were tested:

- LiBackPack C50 [39];
- Kaarta Stencil [40];
- Gexcel Heron Lite [41].

Table 1. Tested MMS.

	LiBackPack C50	Kaarta Stencil	Gexcel Heron Lite
Weight	6.2 kg	1.7 kg	3.3 kg
LiDAR sensor	Velodyne VLP-16	Velodyne VLP-16	Velodyne Puck Lite
Range	1–100 m	1–100 m	1–100 m
Scanning rate	300,000.000 point/s	300,000.000 point/s	300,000.000 point/s
LiDAR precision	±3 cm	±3 cm	±3 cm
Output precision	5 cm	5 cm	5 cm (with loop closure)
FOV	V −15°/+15°; O 360°	V 30°; O 360°	V −15°/+15°; O 360°
Camera	360°	Feature Tracker	-
Storage	512 GB	1 TB	256 GB
Output format	.las, .ply, .LiData	.las, .ply	.las, .ply, .e57

(**a**) (**b**) (**c**)

Figure 4. The three tested MMS: LiBackPack C50 (**a**) Kaarta Stencil (**b**) and Gexcel Heron Lite (**c**).

They were tested on TF1, TF2 and TF3 in order to obtain comparable data. Output data from the three different systems were compared by assuming TLS point clouds as "Ground Truth".

During the survey campaigns, the systems tested were all used by a walking operator, over the same route, and under the same conditions.

Specifically (Figure 5), with the LiBackPack C50, two different survey circuits were performed within TF1 (Figure 5a), and a longer route linking TF1 and TF2 was subsequently employed.

(**a**) (**b**) (**c**)

Figure 5. Survey paths, TF1 (**a**), TF2 (**b**), and TF3 (**c**).

With Kaarta Stencil and Heron Lite, more tests were carried out: the paths regarding TF1 (Figure 5a) were similar to the corresponding paths used with the first tested device; the second route (Figure 5b) investigated Cereri Island (TF2). A further test (Figure 5c) was conducted in TF3, related to the entry, cloister and indoor spaces of the IUAV Terese headquarters (Figure 5).

The last test was conducted using the Kaarta, which was anchored to a substructure attached to a boat (Figure 6). Strong noise and drift faults defined the data produced using this method of investigation; hence, multiple post-processing attempts were made after segmenting the entire point cloud into manageable chunks. The results indicate that noise levels decreased to tolerable levels, especially at the section's edges, but that the problems recalculating and reconstructing the trajectory that result in data drift persist.

Figure 6. Kaarta boat system.

3. Dataset Elaboration and Analysis

Scans generated by the LiBackpack C50, Kaarta Stencil and Heron Lite systems were post-processed using dedicated software (LiDAR360 (GreenValley Interntional, Berkeley, CA, USA), Playback Raw Data (Kaarta, Pittsburgh, PA, USA), Reconstructor (Gexcel srl, Brescia, Italy)). A multi-scan registration process was employed in order to obtain a point cloud for each MMS for every TF.

Then, the final point clouds were geo-referenced using the TLS "Ground Truth". The same reference system was obtained thanks to a manually performed pre-alignment (rough alignment) using the CloudCompare software package, which was subsequently optimised using the ICP algorithm, which improves the accuracy of the alignment at each iteration by randomly examining a subsample of point clouds.

"The ICP method uses an error function to minimise the sum of the squared distances. The equation shows the formula for the error function used in the ICP method" [42].

$$E\ (R,t) = min_{R,t} \sum i||p_i - (Rq_i + t)||^2 \quad (3)$$

where:

- $p_i \in P$: *i-th* point from the reference cloud;
- $q_i \in Q$: *i-th* point from the compared cloud.

The RMS values obtained after the ICP alignment are listed below (Table 2).

Table 2. ICP alignment RMS values.

	TF1	TF2	TF3
LiBackPack C50	0.064 m	-	-
Kaarta Stencil	0.026 m	0.045 m	0.077 m
Heron Lite	0.053 m	0.055 m	0.052 m

3.1. Quantitative Data Comparison

3.1.1. Global Comparison: Cloud-to-Cloud

The focus of the analyses is the comparison of the data processed using the different survey instruments with the aim of verifying their reliability, correctness, and completeness. These comparisons were performed using the CloudCompare software package by means of the C2C and C2M distance calculation method. Both methodologies make it possible to compute the distances between two clouds or between a cloud and a mesh. In all comparisons, 1 m was set as the threshold value.

The C2C computational method is a system based on distance estimation using the Hausdorff algorithm. This algorithm is used to measure the difference between two different representations of the same three-dimensional model. The estimation of the distance from a set of points A to a set of points B is defined as the maximum function, as defined by the following equation [43]:

$$H\ (A,B) = max(h(A,B), h(B,A)) \quad (4)$$

where:

- $h(A,B) = max_{a\ \in\ A} min_{b\ \in\ B} ||a-b||$;
- $h(B,A) = max_{b\ \in\ B} min_{a\ \in\ A} ||a-b||$;
- a: points of the set A;
- b: points of the set B;
- $||a-b||$;: Euclidean distance between points.

The algorithm determines the distance between two points (Figure 7), where the closest point in the compared cloud is found for each point in the reference cloud.

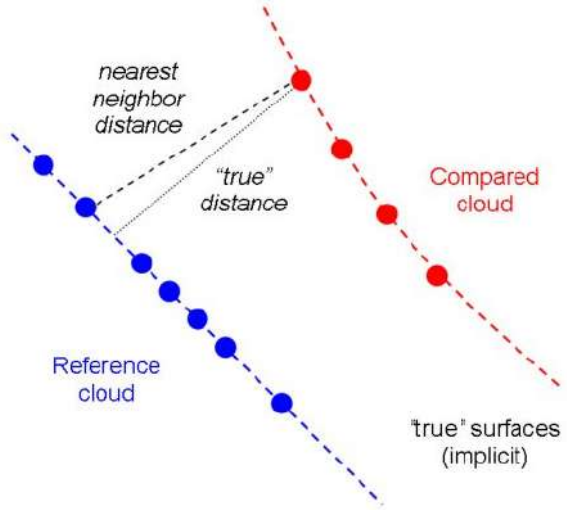

Figure 7. Distance between points.

The same procedure was used to compute the C2M distance, the principle of which involves taking the triangular mesh as a reference model. This implies that the distance is estimated between the vertices of the triangles composing the mesh and the respective points belonging to the compared cloud. The results are presented in Section 4.

3.1.2. Residual Analysis of Control Points

As stated before, the aim of this paper is the morphological study of the Venice urban fabric. A three-dimensional global analysis was set as the main tool for investigating the ability of the SLAM systems to document the relationship between building typology and urban morphology; then, a further quantitative bi-dimensional study was performed in order to evaluate the potential of MMSs to contribute to the realisation of traditional urban cartography and to build bi-dimensional drawings to fill the gap between the urban and architectural scales. Horizontal profiles were extracted from the TLS and MMSs point clouds, and two set of homologous control points were identified on them (Figure 8).

To compare the two sets of coordinates, a rototranslation with scale variation must be performed as a first step, which eliminates the macro-differences between the two sets, thereby bringing the second set of points $(x'_i; y'_i)$ back into the same reference system as the first $(x_i; y_i)$. The so-called Helmert transformation is a global conformal transformation that considers four parameters: translation Δx, translation Δy, rotation α, and scale change λ [44].

$$\begin{bmatrix} x \\ y \end{bmatrix} = \lambda \begin{bmatrix} \cos\alpha & -sen\alpha \\ sen\alpha & \cos\alpha \end{bmatrix} \begin{bmatrix} x' \\ y \end{bmatrix} + \begin{bmatrix} \Delta x \\ \Delta y \end{bmatrix} \quad (5)$$

After obtaining the residuals on the single pairs of coordinates, they were graphically mapped in order to visualise their distribution on the investigated cloud by means of the Surfer 16 software package (Version 16, Golden Software, LLC, Golden, CO, USA).

This software generates a raster image in colour scale (Figure 9) that shows, in a 2D space, the position of the control points analysed and assigns to each point the corresponding value of the residual computed after rototranslation. For all other points (pixels) of the image, the residual values, which are not known, are assigned by interpolation using the Kriging algorithm [45].

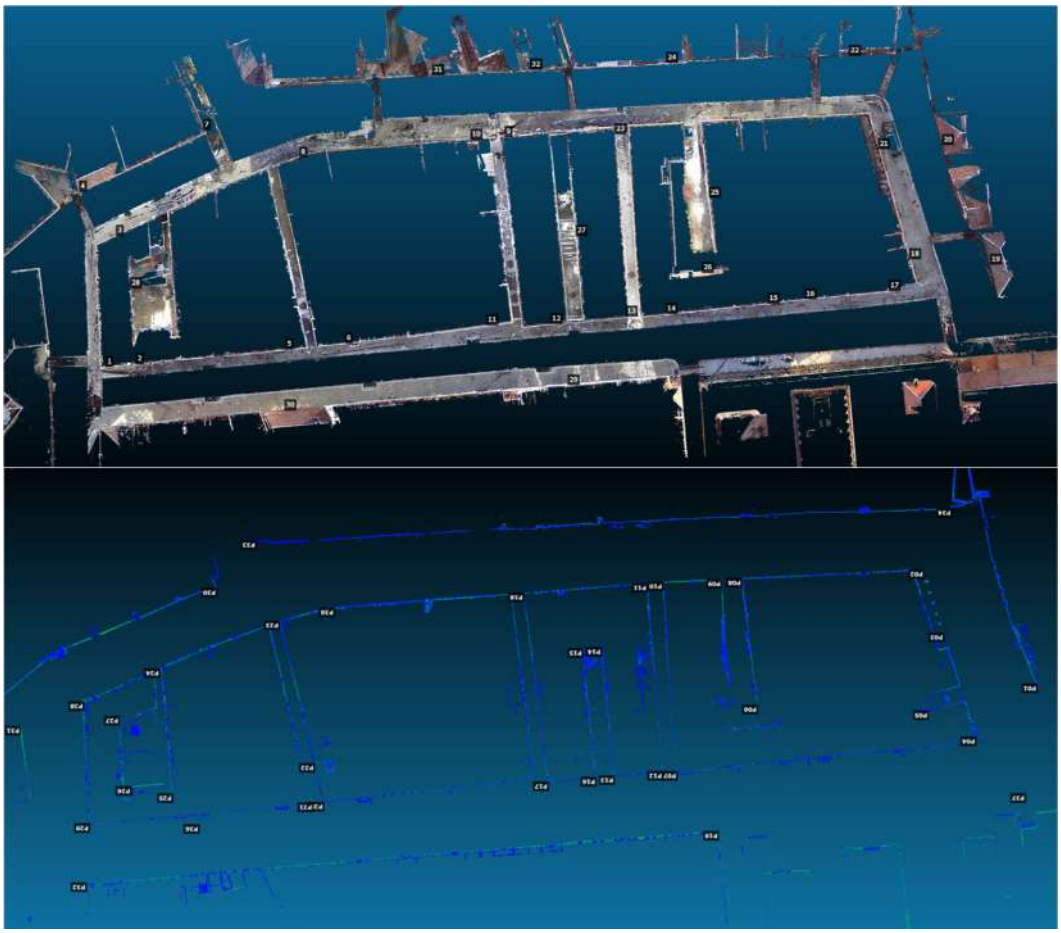

Figure 8. TLS/Kaarta Stencil, identified control points.

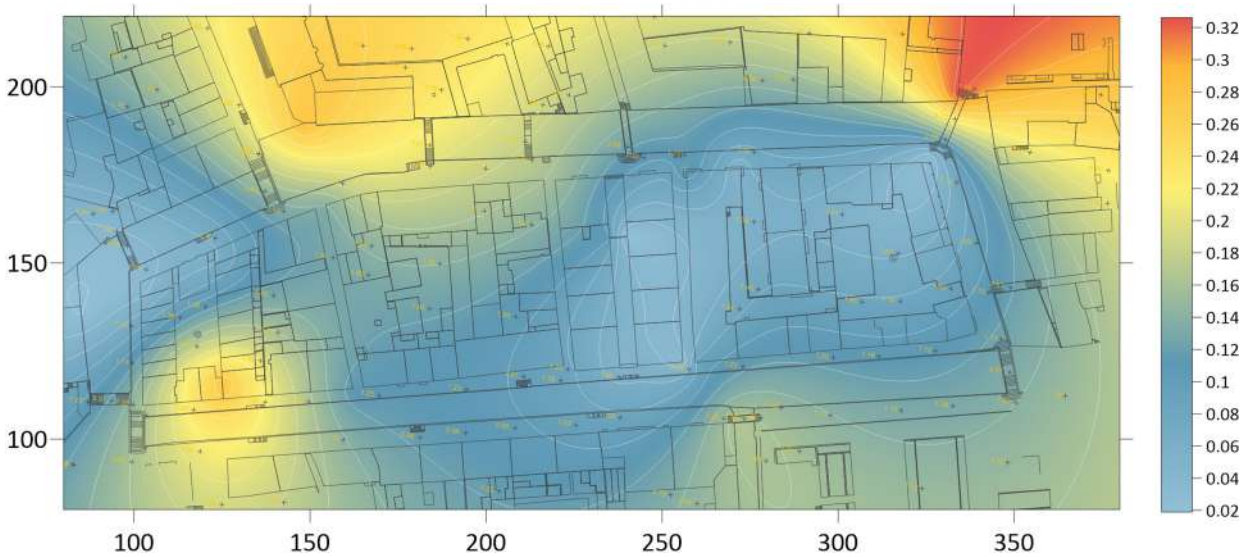

Figure 9. Example of residual distribution: it can be seen that the central part of the example area presents no substantial discrepancies between TLS and MMS data, while two single control points in the upper right and lower left corners have higher residual values (up to 0.3 m) due to misalignments between scans in these areas.

3.1.3. Strain Analysis

This study investigates the local deformations affecting an MMS point cloud compared to one obtained through TLS and to the reference cartographic data on a bidimensional level through the estimation of elastic deformation parameters.

Starting from the SLAM and TLS datasets, the buildings' horizontal profiles were obtained and firstly compared with the current cartography (CTCN 5000 of Comune di Venezia) according to the principles of strain analysis.

The proposed method uses as input data the differences between the coordinates of two sets of points. Before calculating the deformation parameters, a rototranslation with a scale change was applied to the second set of points in order to obtain the best fit with the first set.

Initially, cartography was taken as the reference object, but comparisons revealed a substantial mismatch with the TLS survey, which proved to be more accurate in terms of precision and accuracy.

Therefore, it was decided to use the TLS survey as the "Ground Truth", as it had previously been compared with the topographic coordinates and validated as the most accurate data set among those available (in this case, the mean of the residuals estimated for each pair of control points was equal to 0.013 m).

A decomposition of the dominion into finite elements was carried out starting from the reference cloud control points by means of the Delaunay triangulation (Figure 10), which was then reported on the second cloud to subdivide the investigated area into triangular patches [46].

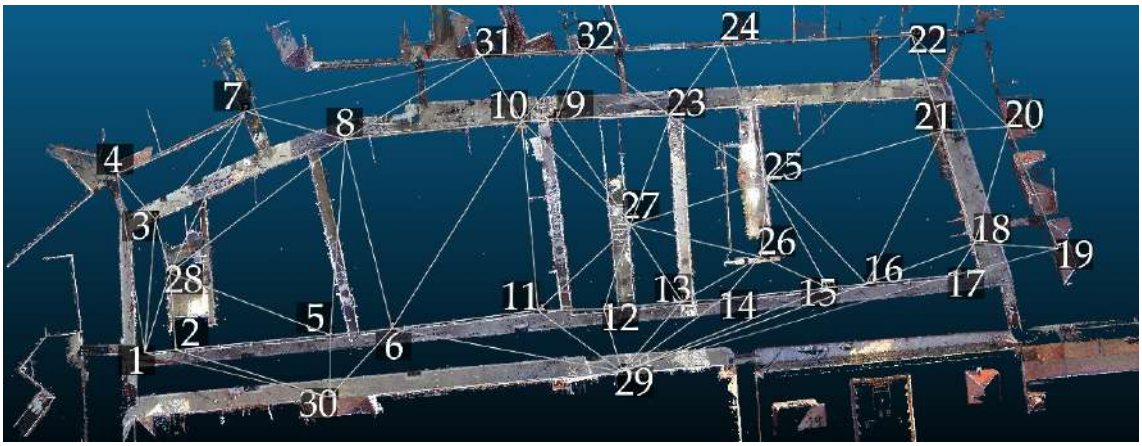

Figure 10. TLS control points and triangulation.

The software package Tensori_3, set up by the IUAV Laboratorio di Fotogrammetria CIRCE (Venice, Italy), which was used to perform the strain analysis, made it possible to calculate the following parameters for each triangle barycentre [47–50]:

E_{max}; E_{min}: eigenvalues of the E matrix, referring to the infinitesimal position (u, v) where:

- U = $x'_i - x_i$; v = $y'_i - y_i$;
- dilatation: Δ E_{max} + E_{min};
- maximum effort: γ $E_{max} - E_{min}$;
- rotational deformation: 12(∂u/∂y − ∂v/∂x);
- azimuth of the axis of maximum tension: ϑarctg(λ2/λ1)/2;
- stress energy dissipated during the deformation process: W = Δ^2 + 1/2 γ^2.

The values of expansion iso-Δ lines, rotation iso-ω lines, and dissipated energy iso-W lines were investigated. This made it possible to locally identify the type of deformation generated by the SLAM instruments.

The Δ expansion represents the isotropic part of the deformation close to the point. The ω rotational deformation describes the infinitesimal rotation due to the deformation and confirms the drift hypothesis. Finally, the strain energy dissipated during the deformation process is a positive scalar that synthesizes the isotropic and anisotropic components of the strain into a single measure.

Starting from the control points, the triangulation performed by the software made it possible to estimate and assign the strain parameters relative to each triangle barycentre. Then, using the Surfer 16 software, the processed data were graphically mapped (Figure 11), and it was possible to draw isolines of equal strain value for each elastic parameter considered. The calculated value was assigned to the barycentre of each triangle, and for the remaining points, the values were obtained by interpolation using the Kriging algorithm.

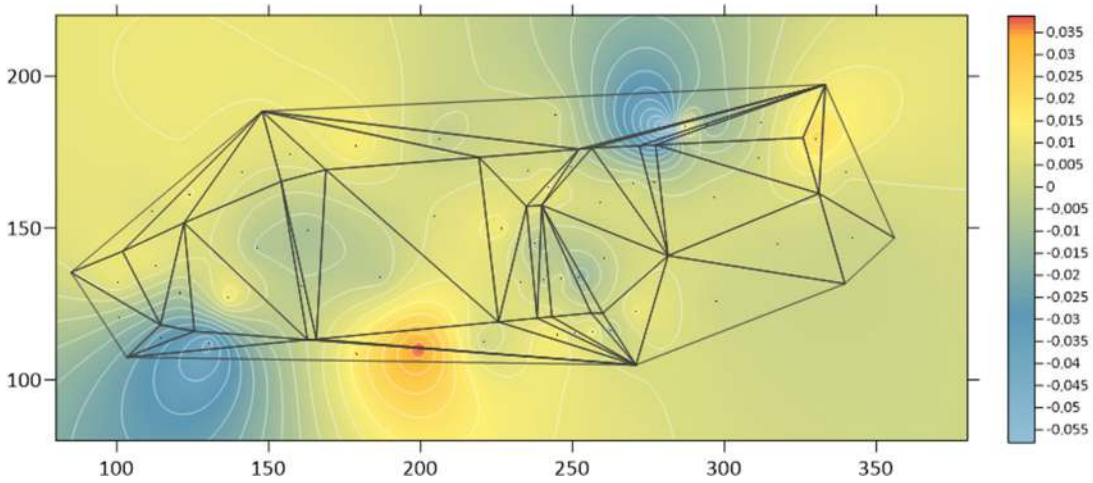

Figure 11. TF2, TLS/Kaarta Stencil.

The comparisons performed with this method for each analysed area are reported below (Table 3).

Table 3. Comparison performed.

Ground Truth	Compared Data
CTCN5000	TLS
Topographic survey	TLS
1:100 Plan	Kaarta Stencil
TLS	LiBackPack C50
TLS	Kaarta Stencil
TLS	Heron Lite

3.2. Qualitative Comparison

Data Quality and Completeness

To obtain a more extensive overview of the performance of the tested systems, several considerations related to the level of data quality, accuracy, and completeness were made.

The main target was to test the reliability of the instruments for the dynamic recording of data within an urban reality. Although all the MMS used during the acquisition phases were equipped with the same Velodyne VLP-16 laser sensor (Velodyne LiDAR, San Jose, CA, USA), the final results appear to be very different from each other. The point densities defining the clouds created by the different systems, computed with the CloudCompare software [51], are tabulated in example form (Table 4).

Table 4. Density values of the clouds created by the different systems.

LiBackPack C50	2978.639/m^2
Kaarta Stencil	14,127.573/m^2
Heron Lite	681.018/m^2
FARO Focus	273,313.671/m^2

The accuracy of the generated 3D model depends greatly on the established scanning range and acquisition angle of the various instruments. In some cases, the greatest difficulties were encountered in the acquisition of the higher parts, as happened with the LiBackPack C50 and Heron Lite systems. Using Kaarta Stencil, it was necessary to run the scanning paths several times, tilting the laser sensor so that it could acquire the tops of the buildings. This refinement approach produced, in some cases, double or "false" surfaces.

For the purposes of the urban morphology study, it was also necessary to evaluate the quality and capabilities of these technologies to be able to optimally perform the transition in scale from architectural level to urban level. Therefore, some tests were performed that included the connecting paths between the internal and external areas belonging to the IUAV Terese headquarters, in order to verify the architectural detail recognition capability. The qualitative considerations of the performed analysis are closely related to the LoD (Level of Detail), which is influenced by the level of noise and the resolution of the model. It follows that, to increase the LoD, and thus obtain greater precision, it is necessary to reduce the speed of movement close to the areas of particular interest.

4. Results

4.1. LiBackPack C50

4.1.1. Data Acquisition and Processing

The instrument was integrated inside a backpack, and this factor led to some disadvantages: the LiDAR sensor could not be tilted, so it was impossible to scan the highest floors of the surveyed buildings, which are completely missing from the final point cloud.

The post-processing phase, carried out using LiDAR360 software, was substantially based on the recalculation and correction of the estimated trajectory and on the realignment of scans. A refinement procedure was carried out, and a noise filter was applied to remove the outliers generated by moving objects.

4.1.2. Dataset Evaluation

The results obtained from the C2C (Figure 12) and C2M comparison with the TLS cloud used as a reference are quantitatively in line with what was reported in the data sheet of the device. The SQM values obtained from the comparisons are listed below (Table 5).

Table 5. SQM values.

	SQM—C2C	**SQM—C2M**
TF1	0.050 m	0.067 m

The examined datasets show geometric inconsistencies with reality. Misalignments are evident, in terms of both plan and elevation, especially in the clouds corresponding to larger areas, where the route insists on paths with porticoes or narrow passages.

The clouds obtained with the LiBackPack system, even where they are geometrically correct, present noise along the vertical and horizontal surfaces. The thickness of the cloud, measured from the extracted profiles, is on average 5–6 cm on simple and linear walls, but reaches 10–12 cm in areas where the profile is more complex (e.g., in the presence of protrusions and mouldings).

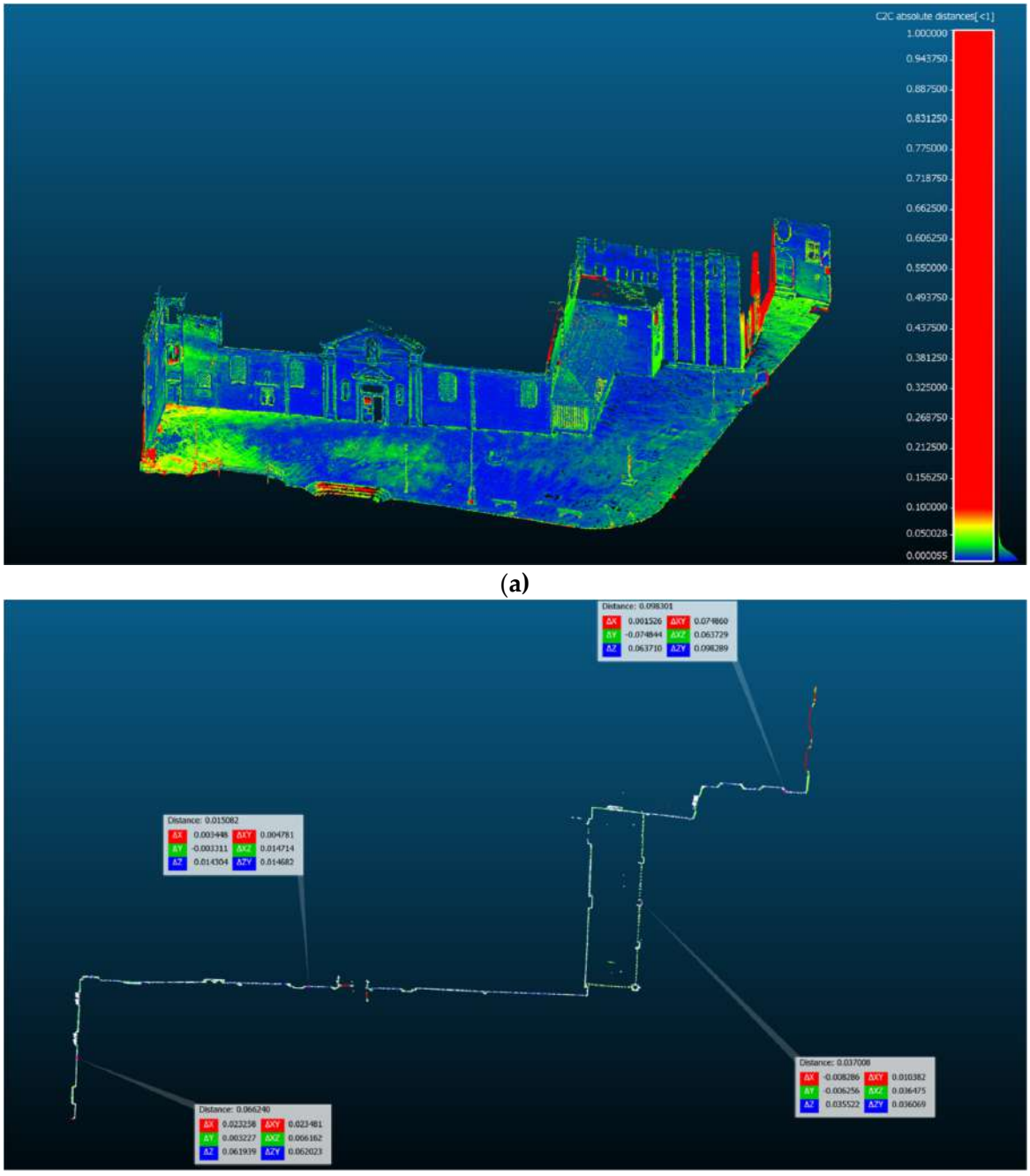

Figure 12. TF1: C2C comparison (**a**), and horizontal section with punctual measurements of the distance between the reference and the compared data (**b**).

Regarding misalignments between the SLAM and TLS clouds, values up to 7 cm are generally measured, although in some areas, presumably as a result of drift error, the distance between the two point clouds is 17–20 cm (Figure 12b).

Concerning residual analysis, four identified points within TF1 have residues greater than 10 cm, the average is 7 cm, and the point with the highest residue (11.5 cm) is located on the facade of the church, corresponding to a double surface generated by the instrument, as already noticed in the C2C comparison (Figure 13).

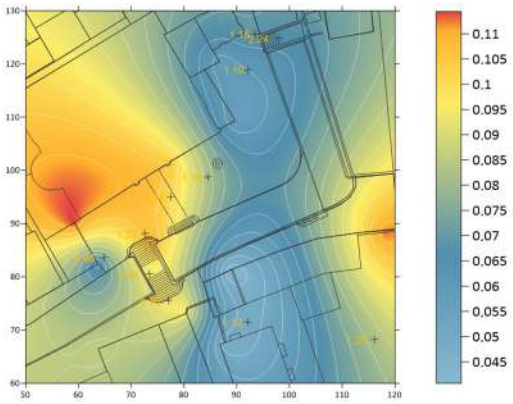

Figure 13. Residuals on homologous points TF1.

Strain analysis results do not show substantial geometrical differences. In terms of expansion, rotation, and dissipated energy, considering the test field of limited dimensions (TF1), it can be observed that the instrument presents minimal anomalies (Figure 14).

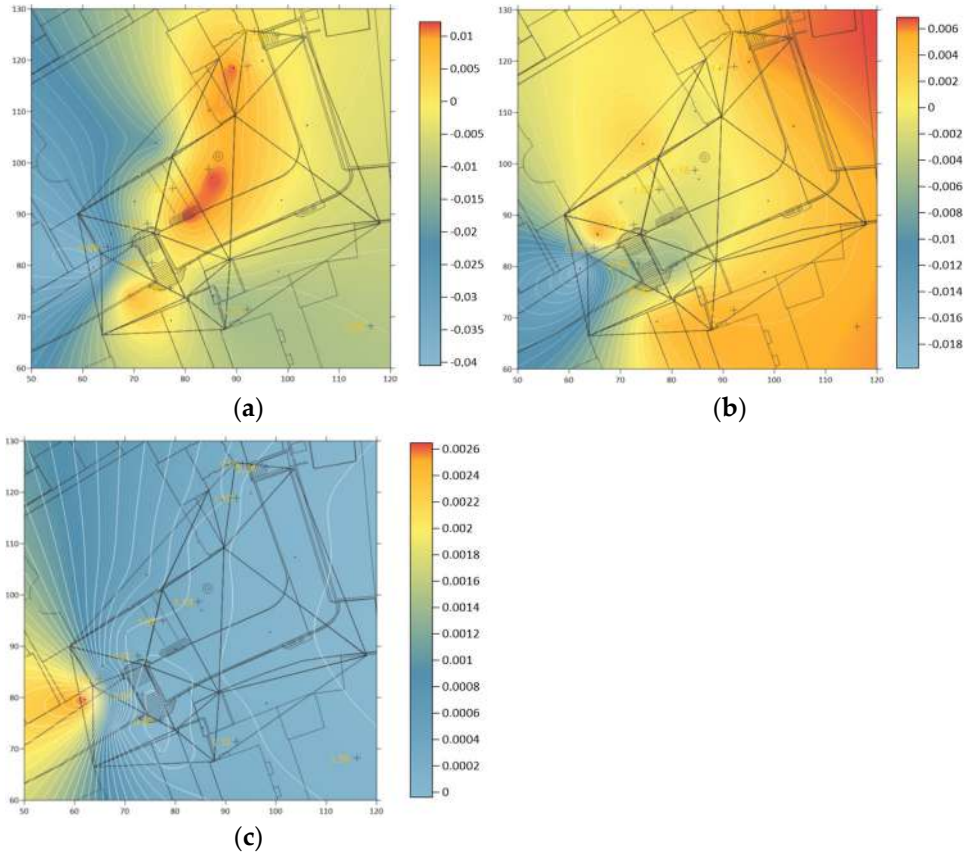

Figure 14. Δ (**a**), ω (**b**), and W (**c**) parameter isolines.

4.2. Kaarta Stencil

4.2.1. Data Acquisition and Processing

During the acquisition phase, there was no need to adopt any particular precautions for the correct working of the instrument, except for maintaining a constant walking speed and performing fluid movements. The LiDAR sensor, carried by the operator, could be tilted with respect to the vertical; this made it possible to acquire information related to the buildings' highest floors, thus resulting in a clearer and more complete point cloud being obtained.

This system acquires and processes data in near real time without the need of complex post-processing for small closed outdoor circuits in which the geometry of the site is not particularly articulated.

Post-processing of the recorded data was necessary to re-compute trajectory elevation and to allow LOAM (LiDAR Odometry And Mapping) algorithms to re-examine the 2D feature recognition to achieve more precise alignment of the indoor scans. In some cases, the obtained clouds presented discrepancies along the vertical component, generating floors tilted up to 25–30° from the horizontal plane.

4.2.2. Dataset Evaluation

The results obtained from the comparison of C2C (Figures 15–17) and C2M with the TLS cloud used as reference are in line with the declarations in the device's data sheet. The differences in extension and geometric complexity of the performed paths were considered and critically evaluated. The values of standard deviation (SQM) obtained for the analysed clouds are listed below (Table 6).

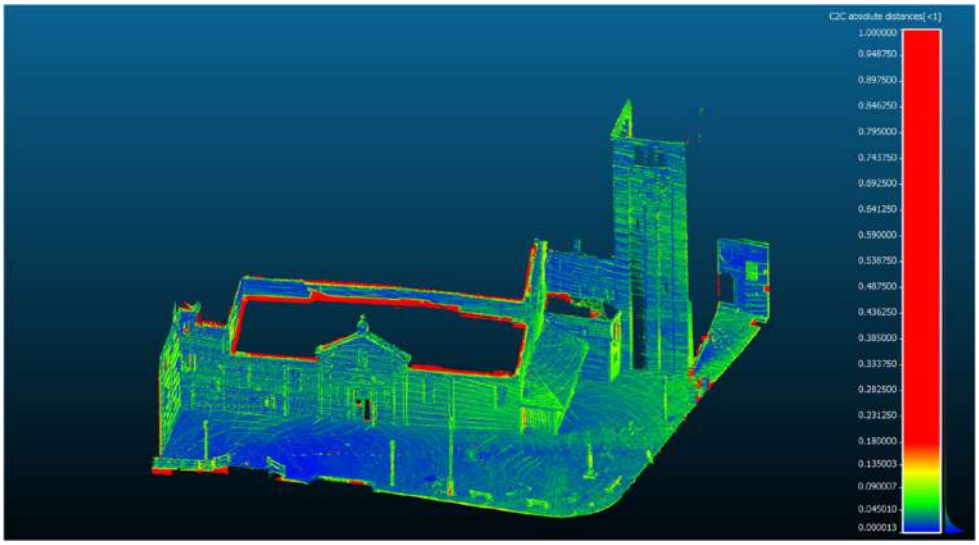

(**a**)

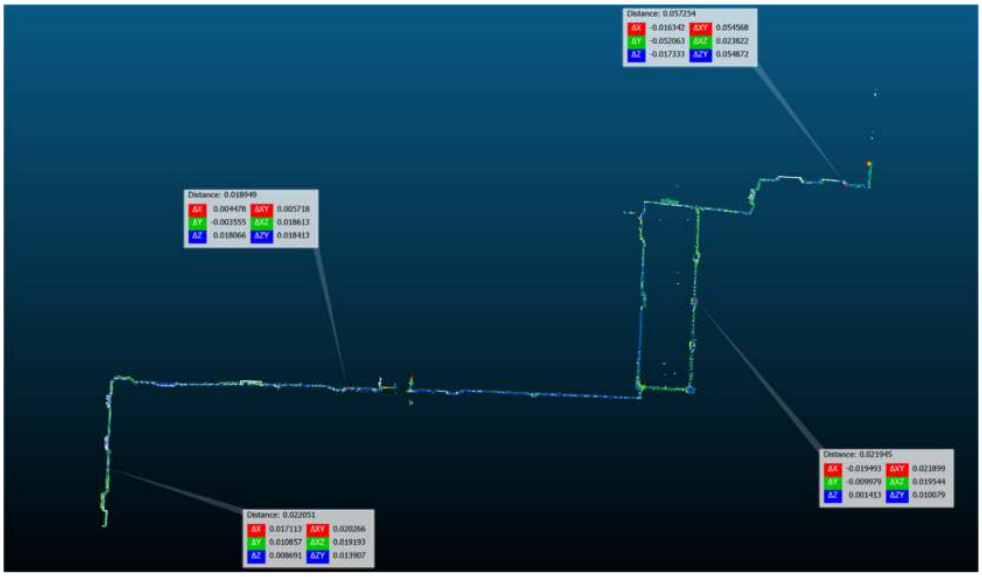

(**b**)

Figure 15. TF1: C2C comparison (**a**), and horizontal section with punctual measurements of the distance between the reference and the compared data (**b**).

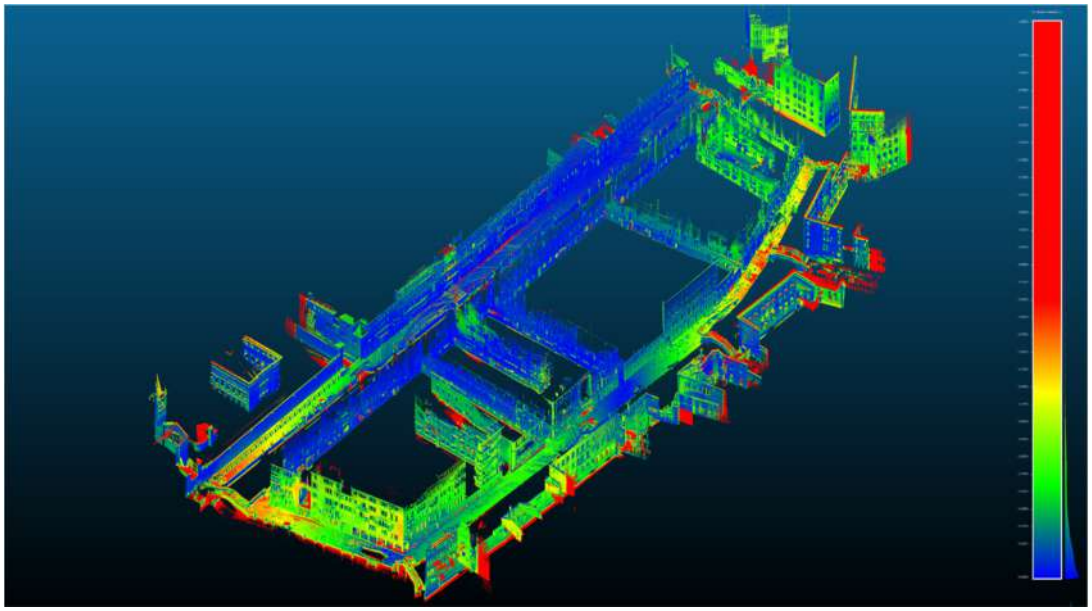

(**a**)

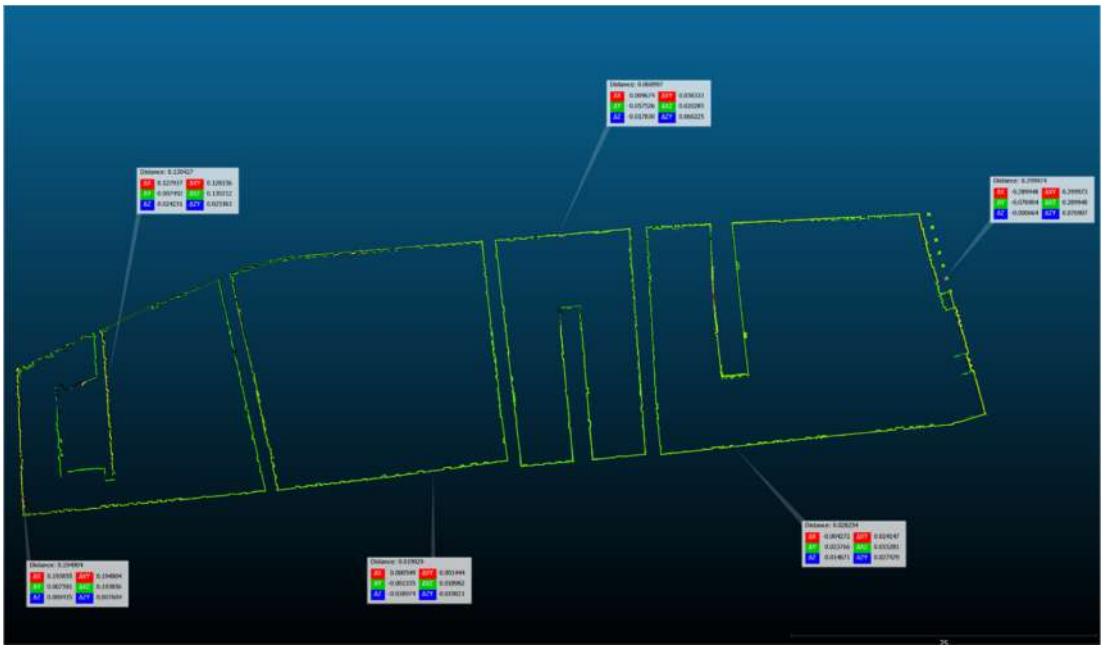

(**b**)

Figure 16. TF2: C2C comparison (**a**), and horizontal section with punctual measurements of the distance between the reference and the compared data (**b**).

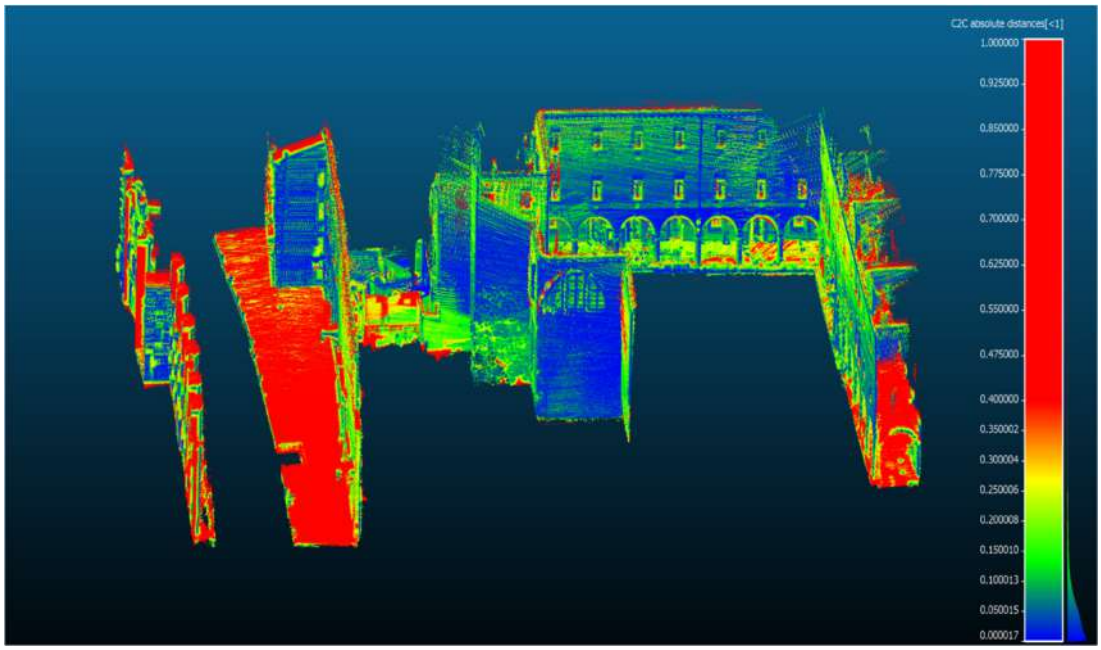

(**a**)

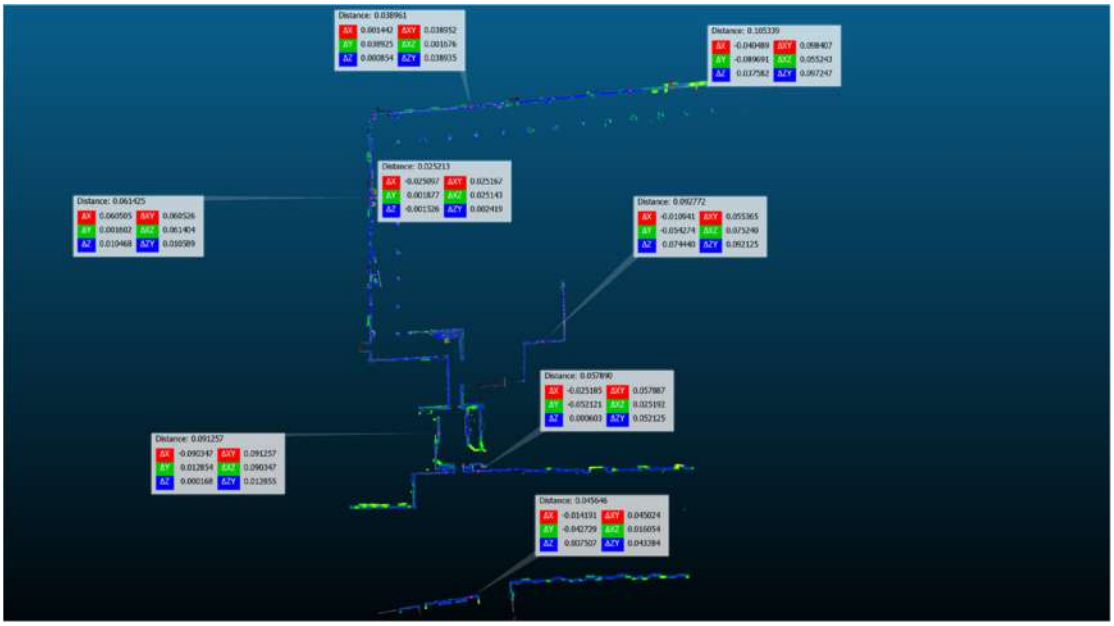

(**b**)

Figure 17. TF3: C2C comparison (**a**), and horizontal section with punctual measurements of the distance between the reference and the compared data (**b**).

Table 6. SQM values.

	SQM—C2C	SQM—C2M
TF1	0.029 m	0.039 m
TF2	0.109 m	0.147 m
TF3	0.097 m	-

For TF2, it was decided to perform an additional C2M comparison. The entire area was divided into three different parts. Three different closed paths were identified, and three point clouds were analysed. This made it possible to partially remove the discrepancies caused by the incorrect alignment of one scan, the error of which had spread over a large number of subsequent scans (Table 7).

Table 7. SQM values.

	SQM—C2M
TF1	0.090 m
TF2	0.092 m
TF3	0.093 m

The three areas identified within TF2 are listed below:

- TF2_01: from Fondamenta de la Madonna to Calle de le Procuratie;
- TF2_02: from Calle de le Procuratie to Calle Cappello;
- TF2_03: from Calle Cappello to Fondamenta San Marco.

Qualitatively, in terms of point density, the Kaarta Stencil clouds seem to be the most complete: the average density is 14,127.573 points/m^2, and the average cloud thickness is 5 cm.

The analysis of the profiles showed different results depending on the examined zone. TF1 presented distances between surfaces ranging from 1 to 5 cm. On TF2, much larger than the previous one, differences of up to 20–25 cm were found at the ends of the cloud, while in the middle part, the two clouds almost overlapped (2 cm). Finally, with respect to TF3, distances between 4 and 10cm were found.

Regarding residual analysis, for TF1, the calculated residuals are generally under 4 cm, but there is a significant geometric difference (9 cm) at the foot of the bridge (Figure 18a).

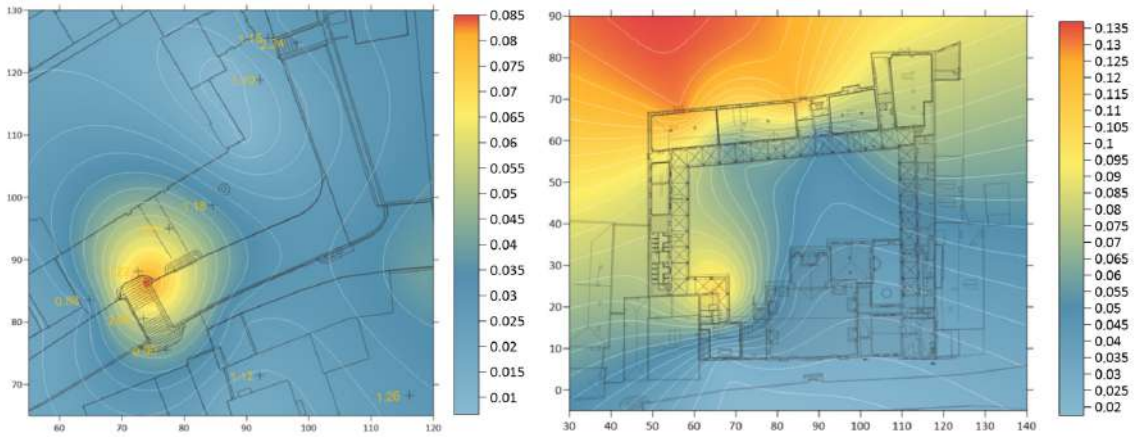

(**a**) (**b**)

Figure 18. Residuals on homologous points TF1 (**a**) and TF3 (**b**).

For TF2, two different analyses were performed: the first (Figure 19a) considered the whole area, with residues below 15 cm and highest values located at the edges of the surveyed region; the second (Figure 19b) excluded from the computation all the points picked outside the insula. Setting a tolerance value of 20 cm, all the observations whose residual values exceeded this quantity were eliminated. This made it possible to obtain lower residuals, which is in line with the 3D global level cloud analysis. The image shows that only three control points present discrepancies between MMS and TLS data (the residuals for these three points are 14.9 cm, 19.7 cm and 18.5 cm).

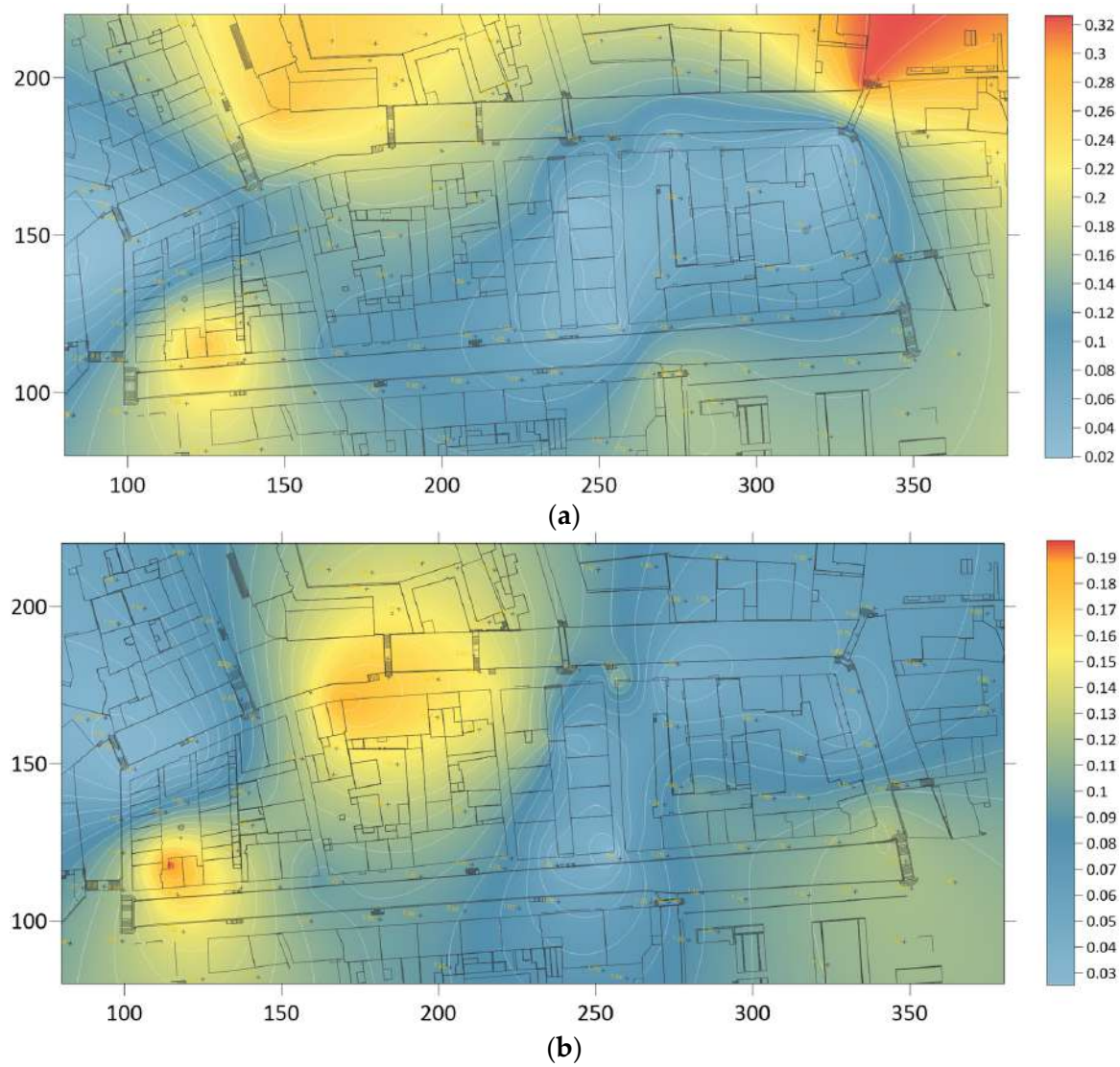

Figure 19. Residuals on homologous points in TF2 in the whole area (**a**) and only the insula (**b**).

Concerning TF3, the results (Figure 18b) show residuals of up to 10 cm for 10 out of 13 control points. These values are in line with the accuracies that can generally be achieved using an MMS system, but with respect to the representation scale required for indoor spaces (1:100–1:200), these results, although good, do not meet the accuracies required.

Relative to strain analysis, the clouds of areas of limited size such as TF1 and TF3 did not show any substantial divergences from the TLS clouds, while the more extended TF2 area presented anomalies. 3D global comparison discrepancies were investigated and confirmed by strain analysis. The three strain parameters showed local anomalies, with misalignments of up to 20–30 cm (Figure 20).

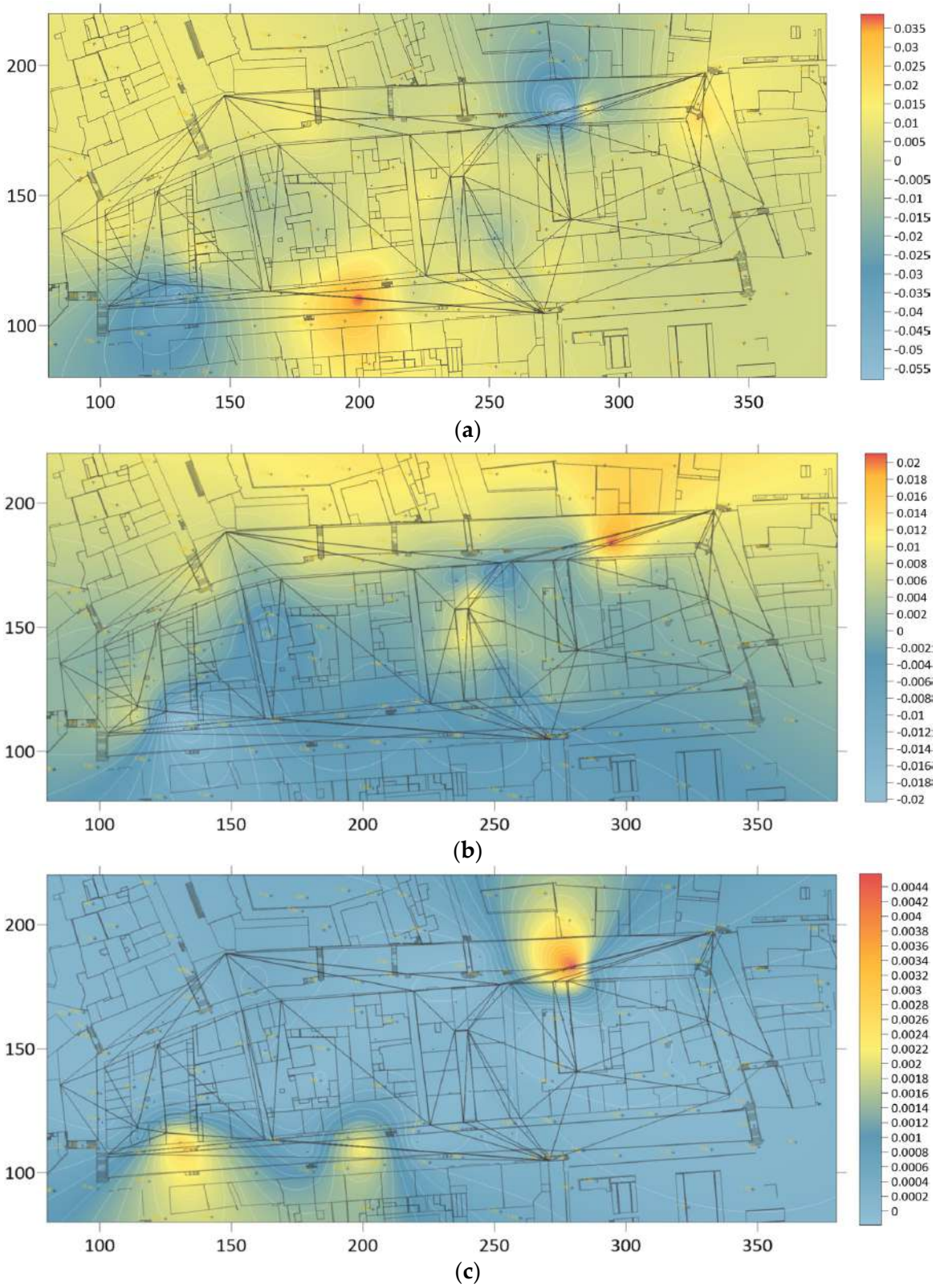

Figure 20. Δ (**a**), ω (**b**), and W (**c**) parameter isolines.

A further strain analysis was carried out, excluding the outermost control points. The new data reduced the presence of this phenomenon, but confirmed the presence of deformations in the lower part of the area on the basis of the misalignments identified by the C2C and C2M comparisons (Figure 21).

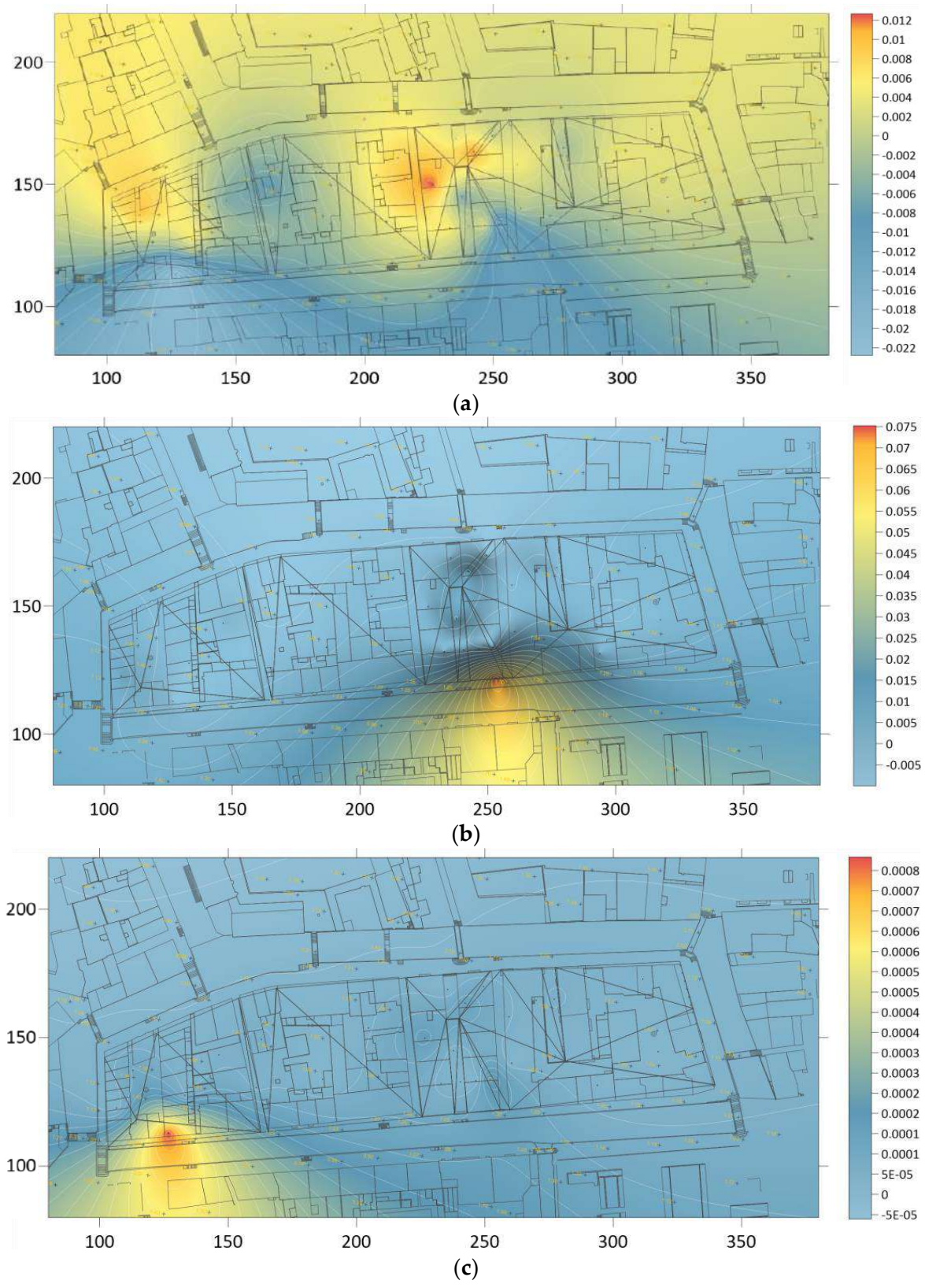

Figure 21. Δ (**a**), ω (**b**), and W (**c**) parameter isolines.

4.3. Heron Lite

4.3.1. Data Acquisition and Processing

This system is the easiest to move and work with. Additionally, in this case, the walking during the acquisition phase was kept as constant as possible in terms of speed, and as fluid as possible in terms of movement. In the post-processing phase, data from this MMS can be integrated with data resulting from a topographic survey. For this reason, every time a topographical point was crossed during the route, a brief stop was made, and the instrument was brought to the ground. This made it possible to geo-reference the cloud on the topographical reference system using the Reconstructor software package.

4.3.2. Dataset Evaluation

Similar to the other tested systems, the data sheet declarations generally reflected what was obtained during the analysis. The standard deviation values obtained from the C2C (Figures 22–24) and C2M comparisons are reported below (Table 8).

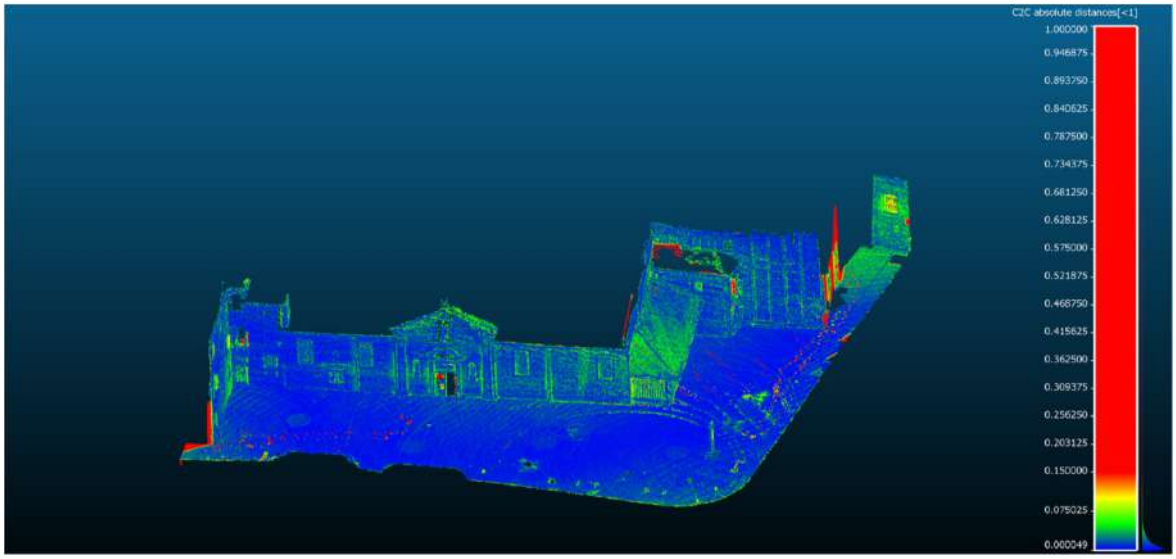

(**a**)

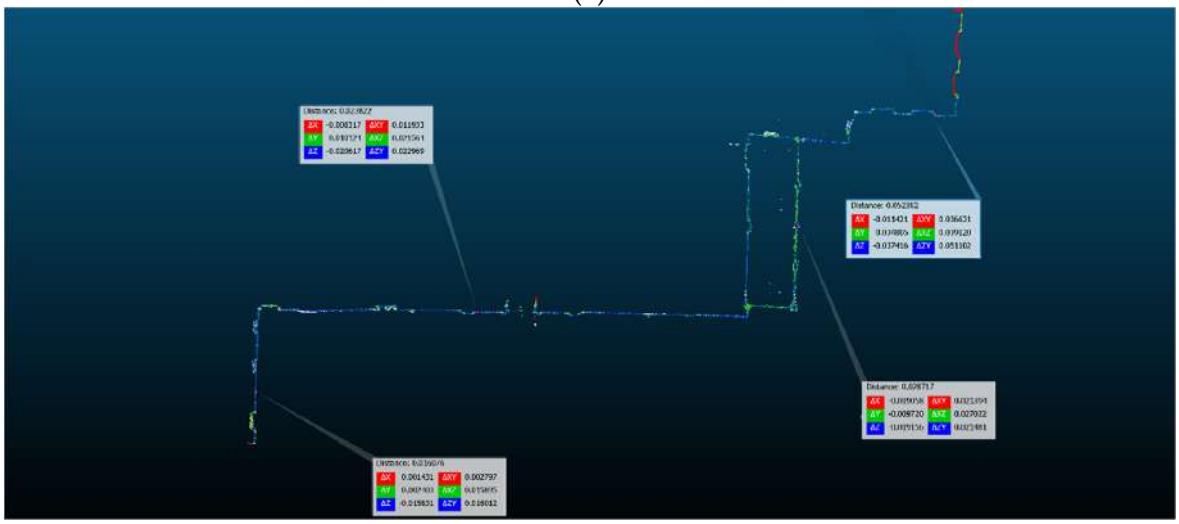

(**b**)

Figure 22. TF1: C2C comparison (**a**), and horizontal section with punctual measurements of the distance between the reference and the compared data (**b**).

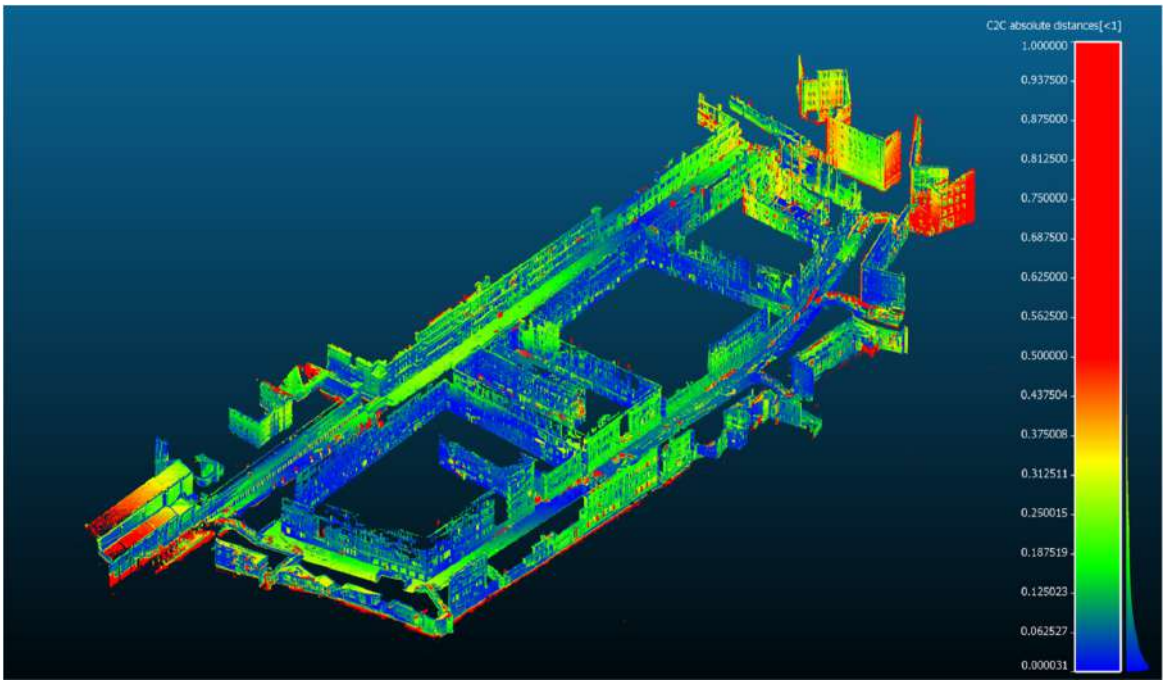

(**a**)

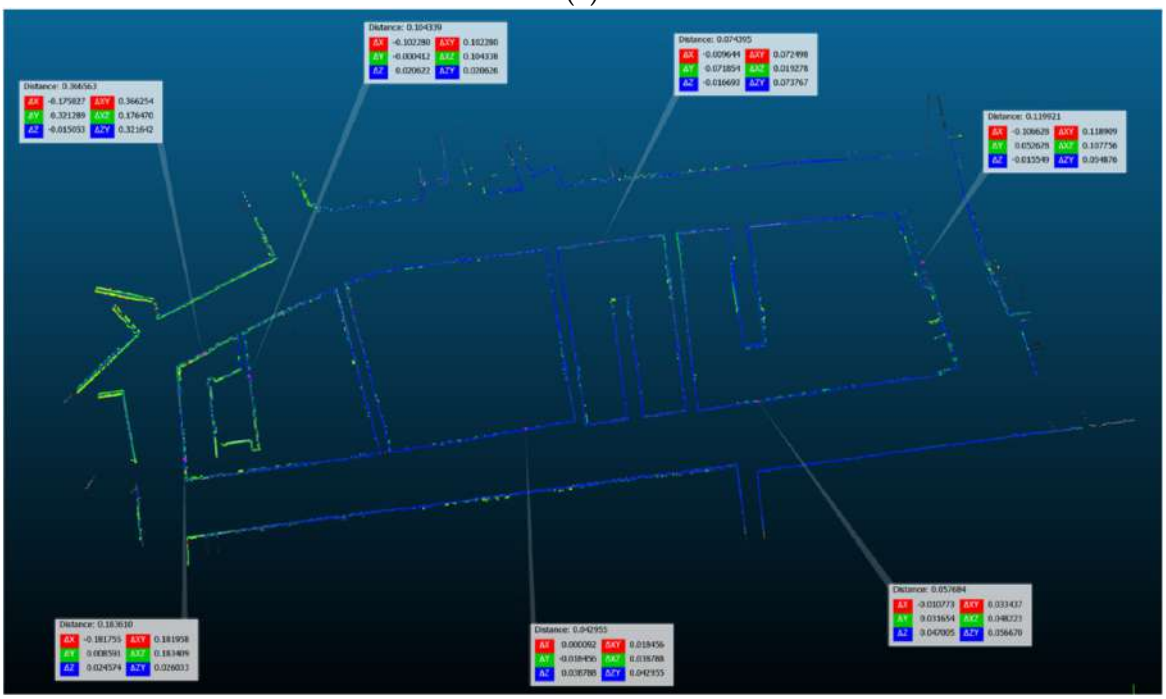

(**b**)

Figure 23. TF2: C2C comparison (**a**), and horizontal section with punctual measurements of the distance between the reference and the compared data (**b**).

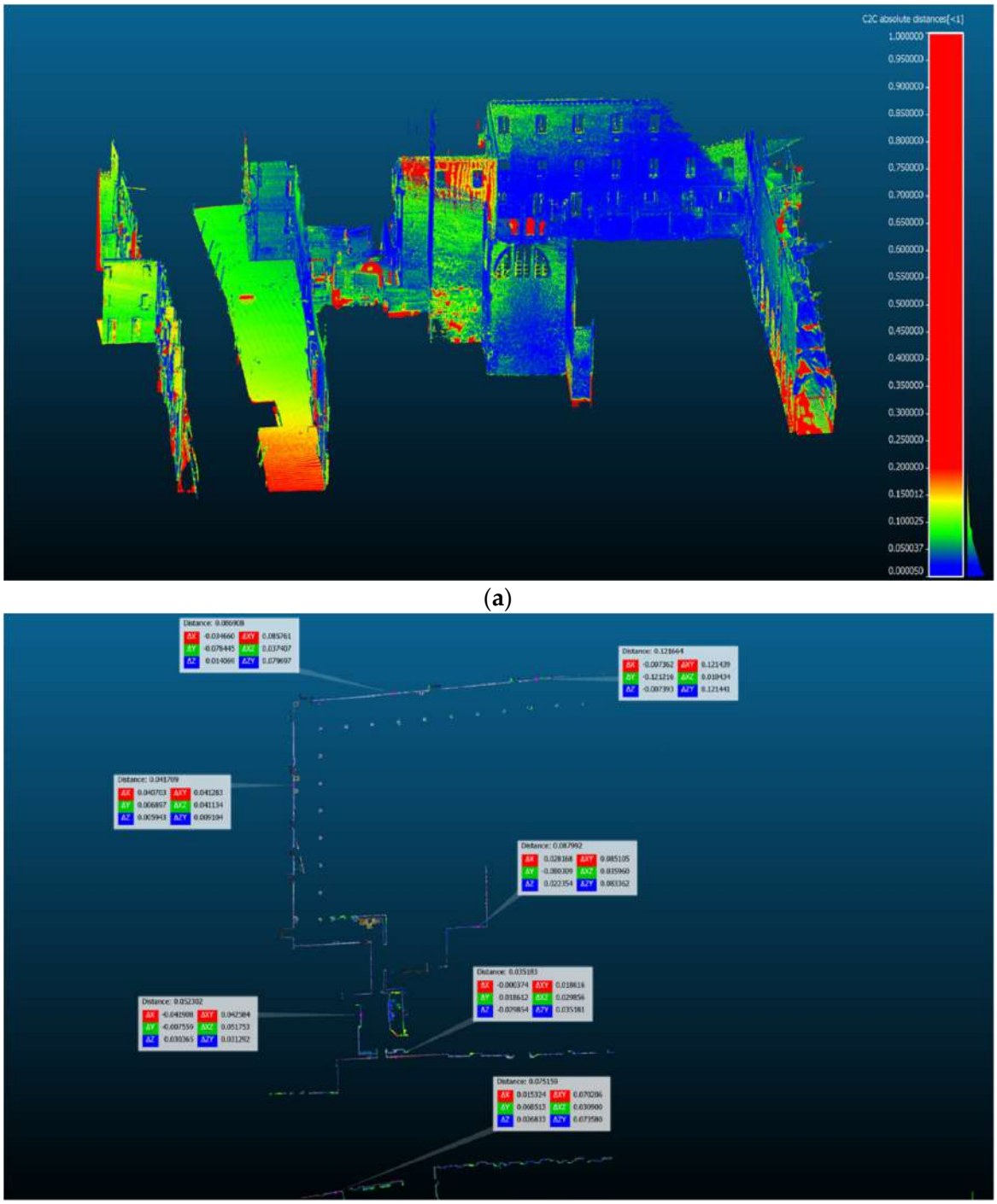

(**a**)

(**b**)

Figure 24. TF3: C2C comparison (**a**), and horizontal section with punctual measurements of the distance between the reference and the compared data (**b**).

Table 8. SQM values.

	SQM—C2C	SQM—C2M
TF1	0.042 m	0.070 m
TF2	0.140 m	0.173 m
TF3	0.075 m	-

The values obtained for TF2, which were much higher than expected, led us to reprocess the dataset (Table 9), performing a recalculation of the trajectory and of the matches identified between the various scans. The zone was subdivided into four smaller areas, listed below:

- TF2_01: from Fondamenta de la Madonna to Calle de le Procuratie;
- TF2_02: from Calle de le Procuratie to Calle Sporca;
- TF2_03: from Calle Sporca to Calle Cappello;
- TF2_04: from Calle Cappello to Fondamenta San Marco.

Table 9. SQM values.

	SQM—C2M
TF2_01	0.132 m
TF2_02	0.090 m
TF2_03	0.088 m
TF2_04	0.083 m

The data obtained from this system are not optimal: the cloud density is very low (681.018 points/m^2), and the lack of RGB values makes it very difficult to recognise architectural details.

The measurement of the distance between the surfaces present in the profiles extracted from the clouds is, in this case, highly variable: 8–9 cm for TF1, 5–30 cm for TF2, and 4–12 cm for TF3.

The residuals on the homologous points, computed by means of residual analysis, are higher. For TF1, the average value is up to 6cm, and the only anomaly (13 cm) is focused on a cloud area that presents a lower density of points and a much greater level of noise (Figure 25a).

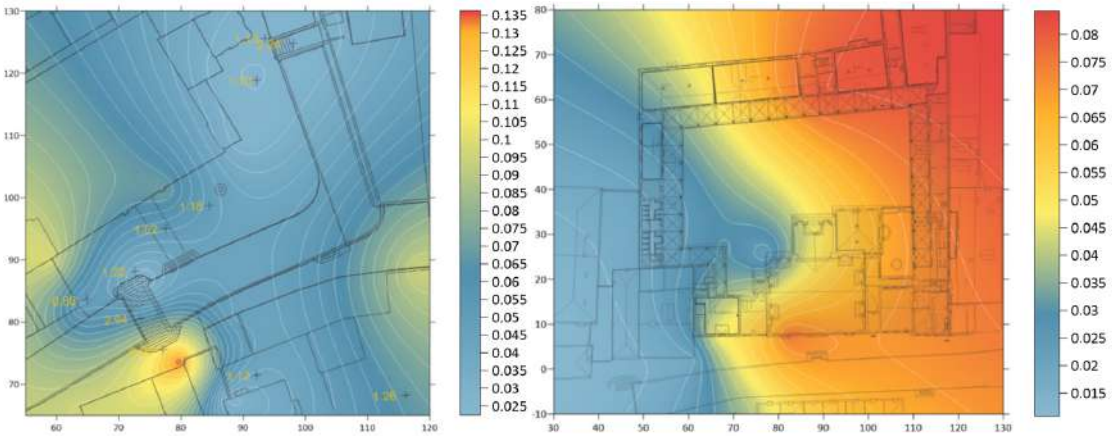

Figure 25. Residuals on homologous points: TF1 (**a**) and TF3 (**b**).

Regarding TF2, most of the residuals computed display values below 15 cm; the greatest inaccuracies were obtained in the area closest to the Rio dei Tre Ponti, which corresponds to the final part of the scanning route employed. The part inside Corte San Marco is also problematic, with a point showing a residual value of 40 cm (Figure 26a). This led to the deletion of observations whose residues exceeded 20 cm, but there was no overall decrease in the results obtained. The residual values of the two points still located within the same area were still very high (39 cm and 41 cm) (Figure 26b).

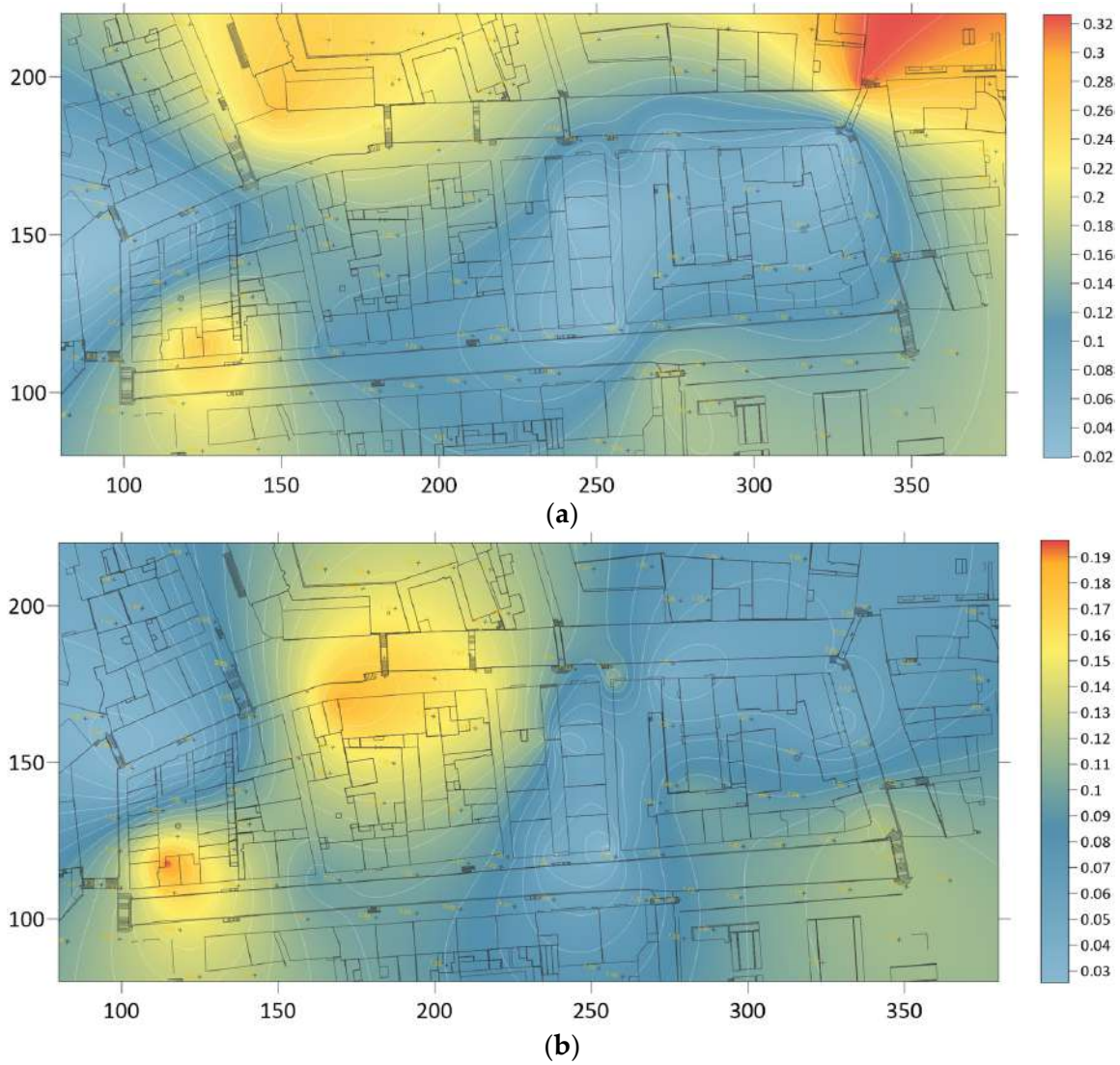

Figure 26. Residuals on homologous points in TF2 in the whole area (**a**) and only the insula (**b**).

For TF3, the conformation of the indoor spaces of the cloister did not allow a homogeneous distribution of control points. On the east side of the building, it was possible to identify only a couple of homologous points, because the cloud was not sufficiently dense and detailed. The uneven distribution of points and the lack of information in that area influenced the final results, and did not allow reliable residual values to be obtained (Figure 25b).

With respect to TF1 and TF3, the strain analysis of the Heron Lite system shows no substantial difference from the two instruments analysed above.

For TF2, the same problems initially observed when using the Kaarta Stencil were found. Therefore, a further strain analysis was carried out strictly considering the insula, with the aim of precisely observing the deformation parameters. In this case, local deformations appeared with a greater frequency (Figure 27).

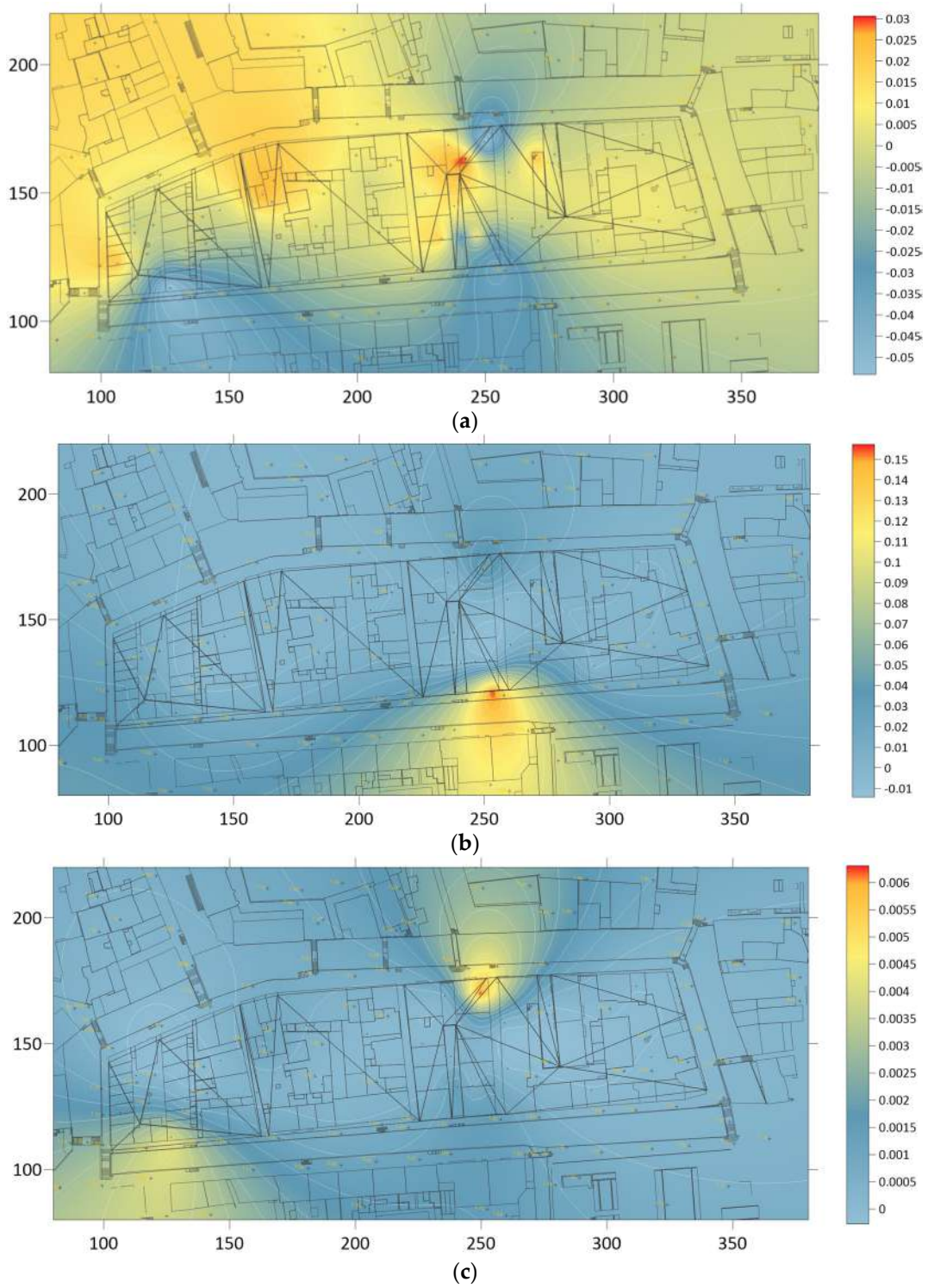

Figure 27. Δ (**a**), ω (**b**), and W (**c**) parameter isolines.

5. Conclusions

SLAM technology implemented in MMS is a surveying method capable of achieving increasingly precise results. The possibility of integrating static surveying instruments with dynamic and versatile products can serve as the basis for much more research in future. The principal aim of the presented investigation was to evaluate the performance and limits of MMS, supported by SLAM technologies, in contributing to the morphological study of the city and giving a geomatic solution to a multidisciplinary typological analysis problem.

Therefore, the analyses dealt with all of the issues related to the mapping of environments, from complex parts of cities to indoor spaces in buildings. Comparisons were performed on the clouds generated by the different MMS by predefining static TLS scans based on topographic measurements as "Ground Truth".

The analyses performed on the data collected during the surveys can be summarised as follows:

- Global analysis: evaluation of the computations of the distances C2C and C2M;
- Evaluation of residual values on control points identified on the compared datasets;
- Local analysis: estimation of elastic deformation parameters using strain analysis.

The results show that the LiBackPack C50, which is practical to use but limited in its movements, creates clouds that are often noisy and which possess a density of points that gradually decreases along the vertical surface. In TF1, where LiBackPack C50 was mainly tested, the presence of many architectural elements with overhangs generated significant misalignments of up to 17 cm compared to the reference TLS cloud, although these were, as shown by the analysis of residual values and deformation parameters, limited to micro-areas where the surface was particularly articulated.

The clouds generated by the Kaarta Stencil proved to be the most accurate and complete; the LOAM technology implemented on this device and the feature-tracking functionality of the integrated camera enabled a solution that was the best among those tested. While for TF1 the comparison between the horizontal profiles showed a difference of 1 to 5 cm compared to the "Ground Truth", in TF2, misalignments of about 20 cm were found at the end of the point cloud. These data, verified and confirmed by the strain analysis, thanks to the expansion and rotation parameters, graphically highlight the critical points, which are located in marginal areas and have residuals of 14.9 cm, 19.7 cm and 18.5 cm, respectively. In the central part, characterised by turns on narrow streets, no discrepancies were found.

The same problems of mismatch on remote areas of the test fields emerged from the point clouds generated by Heron Lite: there are inaccuracies in the same area as for the Kaarta Stencil, with misalignment ranging from 5 cm to 30 cm and residuals of up to 40 cm. The point cloud density was not very high, and had the same problem as the LiBackPack C50, i.e., the gradual decrease in the number of points along vertical surfaces, which were almost incomplete at high elevations. A study of the local deformation parameters confirmed what emerged from the global analysis.

The experimental results based on the data sets collected from each individual instrument made it possible to identify the Kaarta Stencil as being the most suitable MMS system with respect to the aims initially set. The cloud generated by the Kaarta Stencil was then compared with the ground floor of the Terese (TF3). On the basis of this investigation, residuals of less than 10 cm were found for 10 out of 13 control points. Although these results are in line with the MMS analysis, they do not yet satisfy the required accuracy for architectural-scale representation.

With respect to the research goals, our results indicate that all of the tested MMS dealt effectively with the transition between urban and architectural scales, offering datasets capable of containing information linked to the full surveyed area, quickly joining indoor and outdoor environments. Although it still seems difficult to meet the levels of precision required at the architectural level of detail for representation with portable LiDAR systems, it is worth noting that the integration of data derived from other survey techniques can improve the final results; including topographic control points in the post-processing alignment adjustment provides better management of the single scans generated by the MMS, minimising the final error. Only the Heron Lite system is able to deal with this integration at the time of testing, but further software developments are also expected for the other systems.

Therefore, it can be concluded that these technologies have the potential to respond to the targets initially set, but they need further analysis in order to solve technical problems related to the post-processing being performed using different software packages.

Additional and more specific tests on the contribution of expeditious survey techniques to morphological and typological cataloguing have to be carried out, and further analysis is currently ongoing in the same test fields in order to evaluate the possibility of also carrying out 3D strain analysis.

However, it is noteworthy that geomatics, as a result of its continuous technological development, has been able to provide appropriate instruments and techniques in response to specific and multidisciplinary purposes, allowing the development of the groundwork for carrying out an increasingly thorough and precise analysis, and thus contributing to the study of urban morphology.

Author Contributions: Conceptualisation, F.G. and C.B.; Methodology, F.G. and C.B.; Data curation, B.T. and A.M.; Formal analysis, B.T. and A.M.; Supervision, F.G. and C.B.; Validation, F.G., B.T., A.M. and C.B.; Writing—original draft, B.T. and A.M.; Writing—review and editing, F.G., B.T., A.M. and C.B. All authors have read and agreed to the published version of the manuscript.

Funding: This research received no external funding.

Data Availability Statement: Laboratorio di Fotogrammetria CIRCE archives.

Conflicts of Interest: The authors declare no conflict of interest.

References

1. Nocerino, E.; Rieke-Zapp, D.H.; Trinkl, E.; Rosenbauer, R.; Farella, E.M.; Morabito, D.; Remondino, F. Mapping VIS and UVL imagery on 3D geometry for non-invasive, non-contact analysis of a vase. *Int. Arch. Photogramm. Remote Sens. Spat. Inf. Sci.* **2018**, *XLII-2*, 773–780. Available online: https://www.int-arch-photogramm-remote-sens-spatial-inf-sci.net/XLII-2/773/2018/ (accessed on 1 July 2022). [CrossRef]
2. Calantropio, A.; Patrucco, G.; Sammartano, G.; Teppati Losè, L. Sensori low-cost per il mapping speditivo di Beni Culturali. Primi test su di una steadycam low-cost. *Boll. Della Soc. Ital. Fotogramm. Topogr.* **2017**, *3*, 15–24.
3. Bitelli, G.; Gatta, G.; Girelli, V.A.; Vittuari, L.; Zanutta, A. Integrated methodologies for the 3D Survey and the structural monitoring of industrial archaeology: The case of the Casalecchio di Reno Sluice, Italy. *Int. J. Geophys.* **2011**, *2011*, 874347. [CrossRef]
4. Rivolta, M.B.; Rossari, A. *Alexander Klein: Lo Studio Delle Piante e La Progettazione Degli Spazi Negli Alloggi Minimi; Scritti e Progetti Dal 1906 Al 1957*; Mazzotta Editore: Milano, Italy, 1957.
5. Muratori, S. *Architettura e Civiltà in Crisi*; Centro Studi di Storia Urbanistica: Roma, Italy, 1963.
6. Rossi, A. *L'architettura Della Città*; Il Saggiatore: Milan, Italy, 1995.
7. Canella, G. *Sulle Trasformazioni Tipologiche Degli Organismi Architettonici*; Libraccio Editore: Monza, Italy, 1965.
8. Caja, M.; Malcovati, S.; Landsberger, M. *Tipologia Architettonica e Morfologica Urbana. Il Dibattito Italiano. Antologia 1960–1980*; Libraccio Editore: Monza, Italy, 2012.
9. Cristinelli, G. *Cannaregio. Un Sestiere di Venezia. La Forma Urbana, L'assetto Edilizio, Le Architetture*; Officina Edizioni: Roma, Italy, 1987.
10. Trincanato, E.R. *Venezia Minore*; Edizioni del Milione: Milano, Italy, 1948; p. 44.
11. Sammartano, G.; Spanò, A. Point clouds by SLAM-based mobile mapping systems: Accuracy and geometric content validation in multisensor survey and stand-alone acquisition. *Appl. Geomat.* **2018**, *10*, 317–339. [CrossRef]
12. Ridene, T.; Goulette, F.; Chendeba, S. Feature-Based Quality Evaluation of 3D Point Clouds—Study of the Per-formance of 3D Registration Algorithms. *Int. Arch. Photogramm. Remote Sens. Spat. Inf. Sci* **2013**, *XL-2/W2*, 59–64. [CrossRef]
13. Toschi, I.; Rodríguez-Gonzálvez, P.; Remondino, F.; Minto, S.; Orlandini, S.; Fuller, A. Accuracy evaluation of a mobile mapping system with advanced statistical methods. *Int. Arch. Photogramm. Remote Sens. Spat. Inf. Sci.* **2015**, *40*, 245. [CrossRef]
14. Abbate, E.; Sammartano, G.; Spanò, A. Prospective upon Multi-Source Urban Scale Data for 3d Documentation and Monitoring of Urban Legacies. *Int. Arch. Photogramm. Remote Sens. Spat. Inf. Sci.* **2019**, *42*, 11–19. [CrossRef]
15. Teppati Losè, L.; Chiabrando, F.; Giulio Tonolo, F. Documentation of Complex Environments Using 360° Cameras. The Santa Marta Belltower in Montanaro. *Remote Sens.* **2021**, *13*, 3633. [CrossRef]
16. Thomson, C.; Apostolopoulos, G.; Backes, D.; Boehm, J. Mobile laser scanning for indoor modelling. *Int. Arch. Photogramm. Remote Sens. Spat. Inf. Sci.* **2013**, *II-5/W2*, 289–293. [CrossRef]
17. Lehtola, V.V.; Kaartinen, H.; Nüchter, A.; Kaijaluoto, R.; Kukko, A.; Litkey, P.; Honkavaara, E.; Rosnell, T.; Vaaja, M.T.; Virtanen, J.-P.; et al. Comparison of the Selected State-Of-The-Art 3D Indoor Scanning and Point Cloud Generation Methods. *Remote Sens.* **2017**, *9*, 796. [CrossRef]
18. Masiero, A.; Fissore, F.; Guarnieri, A.; Piragnolo, M.; Vettore, A. Comparison of low cost photogrammetric survey with TLS and Leica Pegasus backpack 3D models. *Int. Arch. Photogramm. Remote Sens. Spat. Inf. Sci.* **2017**, *42*, 147–153. [CrossRef]
19. Puente, I.; González-Jorge, H.; Martínez-Sánchez, J.; Arias, P. Review of mobile mapping and surveying technologies. *Measurement* **2013**, *46*, 2127–2145. [CrossRef]

20. Nocerino, E.; Menna, F.; Remondino, F.; Toschi, I.; Rodríguez-Gonzálvez, P. Investigation of indoor and outdoor per-formance of two portable mobile mapping systems. In Proceedings of the Proc. SPIE 10332, Videometrics, Range Imaging, and Applications XIV, Munich, Germany, 26 June 2017; Volume 103320. [CrossRef]
21. Dewez, T.J.B.; Plat, E.; Degas, M.; Richard, T.; Pannet, P.; Thuon, Y.; Lucas, J. Handheld mobile laser scanners Zeb-1 and Zeb-Revo to map an underground quarry and its above-ground surroundings. In Proceedings of the Virtual Geosciences Conference: VGC, Bergen, Norway, 22–23 September 2016.
22. Farella, E.M. Rilievo tridimensionale di ambienti ipogei con un sistema a scansione laser portatile. *Boll. Della Soc. Ital. di Fotogramm. e Topogr.* **2016**, *2*, 1–10.
23. Rodríguez-Gonzálvez, P.; Fernández-Palacios, B.J.; Muñoz-Nieto, A.L.; Arias-Sanchez, P.; Gonzalez-Aguilera, D. Mobile LiDAR system: New possibilities for the documentation and dissemination of large cultural heritage sites. *Remote Sens.* **2017**, *9*, 189. [CrossRef]
24. Zlot, R.; Bosse, M.; Greenop, K.; Jarzab, Z.; Juckes, E.; Roberts, J. Efficiently capturing large, complex cultural heritage sites with a handheld mobile 3D laser mapping system. *J. Cult. Herit.* **2014**, *15*, 670–678. [CrossRef]
25. Farella, E.; Menna, F.; Nocerino, E.; Morabito, D.; Remondino, F.; Campi, M. Knowledge and valorization of historical sites through 3d documentation and modelling. *Int. Arch. Photogramm. Remote Sens. Spat. Inf. Sci.* **2016**, *41*, 255–262. [CrossRef]
26. Di Stefano, F.; Torresani, A.; Farella, E.M.; Pierdicca, R.; Menna, F.; Remondino, F. 3D Surveying of Underground Built Heritage: Opportunities and Challenges of Mobile Technologies. *Sustainability* **2021**, *13*, 3289. [CrossRef]
27. Calantropio, A.; Chiabrando, F.; Spanò, A. Impiego di tecniche di fotogrammetria digitale speditiva a supporto delle opere provvisionali negli interventi tecnici in emergenza sismica. *Boll. Della Soc. Ital. di Fotogramm. e Topogr.* **2018**, *3*, 22–31.
28. Muratori, S. Studi per una operante storia urbana di Venezia. *Roma Ist. Poligr. Dello Stato Libr. Dello Stato.* **1960**, *6*, 99.
29. Wang, R.; Peethambaran, J.; Chen, D. LiDAR Point Clouds to 3-D Urban Models: A Review. *IEEE J. Sel. Top. Appl. Earth Obs. Remote Sens.* **2018**, *11*, 606–627. [CrossRef]
30. Taheri, H.; Xia, Z.C. SLAM; definition and evolution. *Eng. Appl. Artif. Intell.* **2021**, *97*, 104032. [CrossRef]
31. Khairuddin, A.R.; Talib, M.S.; Haron, H. Review on simultaneous localization and mapping (SLAM). In Proceedings of the 2015 IEEE International Conference on Control System, Computing and Engineering (ICCSCE), Penang, Malaysia, 27–29 November 2015; pp. 85–90. [CrossRef]
32. Piniotis, G.; Soile, S.; Bourexis, F.; Tsakiri, M.; Ioannidis, C. Experimental assessment of 3d narrow space mapping technologies. *Int. Arch. Photogramm. Remote Sens. Spat. Inf. Sci.* **2020**, *43*, 149–156. [CrossRef]
33. Lauterbach, H.; Borrmann, D.; Heß, R.; Eck, D.; Schilling, K.; Nüchter, A. Evaluation of a Backpack-Mounted 3D Mobile Scanning System. *Remote Sens.* **2015**, *7*, 3753. [CrossRef]
34. Tucci, G.; Visintini, D.; Bonora, V.; Parisi, E.I. Examination of indoor mobile mapping systems in a deversified inter-nal/external test field. *Appl. Sci.* **2018**, *8*, 401. [CrossRef]
35. He, G.; Yuan, X.; Zhuang, Y.; Hu, H. An Integrated GNSS/LiDAR-SLAM Pose Estimation Framework for Large-Scale Map Building in Partially GNSS-Denied Environments. *IEEE Trans. Instrum. Meas.* **2021**, *70*, 1–9. [CrossRef]
36. Albrecht, A.; Heide, N. Mapping and Automatic Post-Processing of Indoor Environments by Extending Visual SLAM. In Proceedings of the 2018 International Conference on Audio, Language and Image Processing (ICALIP), Shanghai, China, 8–25 May 2018; pp. 327–332. [CrossRef]
37. Konecny, J.; Prauzek, M.; Hlavica, J. ICP Algorithm in Mobile Robot Navigation: Analysis of Computational Demands in Embedded Solutions. *IFAC-PapersOnLine* **2016**, *49*, 396–400. [CrossRef]
38. Karam, S.; Lehtola, V.; Vosselman, G. Simple loop closing for continuous 6DOF LIDAR&IMU graph SLAM with planar features for indoor environments. *ISPRS J. Photogramm. Remote Sens.* **2021**, *181*, 413–426. [CrossRef]
39. LiBackPack C50. Available online: https://www.lidar-italia.it/wp-content/uploads/2019/11/LiBackpack-C50.pdf (accessed on 8 June 2022).
40. Kaarta Stencil 2–16. Available online: https://www.kaarta.com/wp-content/uploads/Stencil_2-16_spec_sheet_04.21-web.pdf (accessed on 8 June 2022).
41. Gexcel Heron Lite. Available online: https://gexcel.it/images/soluzioni/HERON/2021_HERON-LITE_Datasheet.pdf (accessed on 8 June 2022).
42. Ahmad Fuad, N.; Yusoff, A.R.; Ismail, Z.; Majid, Z. Comparing the performance of point cloud registration methods for landslidemonitoring using mobile laser scanning data. *Int. Arch. Photogramm. Remote Sens. Spat. Inf. Sci.* **2018**, *42*, 11–21. Available online: https://www.int-arch-photogramm-remote-sens-spatial-inf-sci.net/XLII-4-W9/11/2018/ (accessed on 1 July 2022). [CrossRef]
43. Franci, R.; Parenti-Castelli, V. Sulla qualità di rappresentazione di oggetti approssimati mediante primitive sferiche. In *Progress Report 125*; DIEM–Faculty of Mechanical Engineering, University of Bologna: Bologna, Italy, 2006.
44. Watson, G.A. Computing Helmert transformations. *J. Comput. Appl. Math.* **2006**, *197*, 387–394. [CrossRef]
45. Erdogan, S. A comparision of interpolation methods for producing digital elevation models at the field scale. *Earth Surf. Process. Landf.* **2009**, *34*, 366–376. [CrossRef]
46. Balletti, C.; Calzavara, M.; Guerra, F.; Mazzanti, M. Walking through historical maps of Venice. *e-Perimetron* **2013**, *8*, 200–208.
47. Boutoura, C.; Livieratos, E. Strain analysis for geometric comparisons of maps. *Cartogr. J.* **1986**, *23*, 27–34. [CrossRef]

48. Dermanis, A.; Livieratos, E. Applications of deformation analysis in geodesy and geodynamics. *Rev. Geosphys.* **1983**, *21*, 41–50. [CrossRef]
49. Adami, A.; Balletti, C.; Guerra, F.; Monti, C. Lafrery's perspective map of Milan (1573): Genesis and geometric content. *e-Perimetron* **2011**, *6*, 12.
50. Guerra, F.; Balletti, C. Strain analysis to test historical survey. In Proceedings of the XXIII International Symposium CIPA, Prague, Czech Republic, 12–16 September 2011.
51. CloudCompare Wiki. Available online: https://www.cloudcompare.org/doc/wiki/index.php/Density (accessed on 8 June 2022).